Flood detection using ScanSAR imagery - A case study in Pakistan

Masanobu Shimada

ALOS Science Manager
Earth Observation Research Center
Japan Aerospace Exploration Agency
Sengen 2-1-1, Tsukuba, Ibaraki, Japan, 305-8505
Tel: 050-3362-4489, Fax:029-868-2961, e-mail: shimada.masanobu@jaxa.jp

ScanSAR and Strip SAR

Wide-swath and low resolution vs.
Narrow-swath and high resolution

Swath	350km	<->	70km
Resolution	100m	<->	10m

ScanSAR preserves sensitivity and the resolution.

1995 to 2009 Forest Change in South America

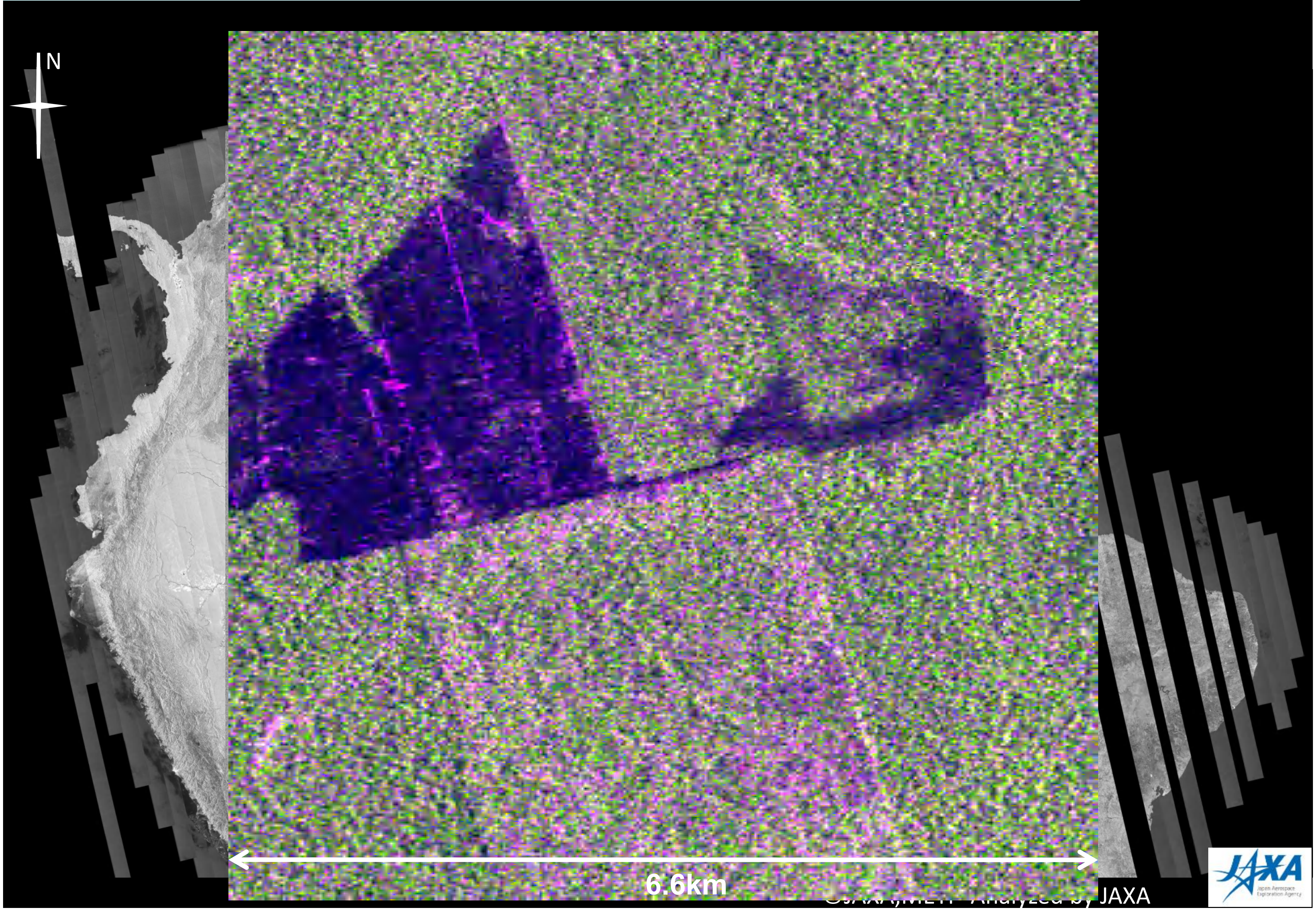

•Environmental monitoring (including the disaster, forest, climate) has been a very important issue.

•Spaceborne SAR has become a stable sensor.

•Geophysical parameter estimation, quick provisions, and large scale information are required.

ALOS

Launch Date	2006/1/24
Launcher	H-IIA-8
Mass	4,000kg
Solar Power	7kW
Orbit	Sun synchronous
Height	691.65km
Revolution (Sub-Cycle)	46 days (2 days)

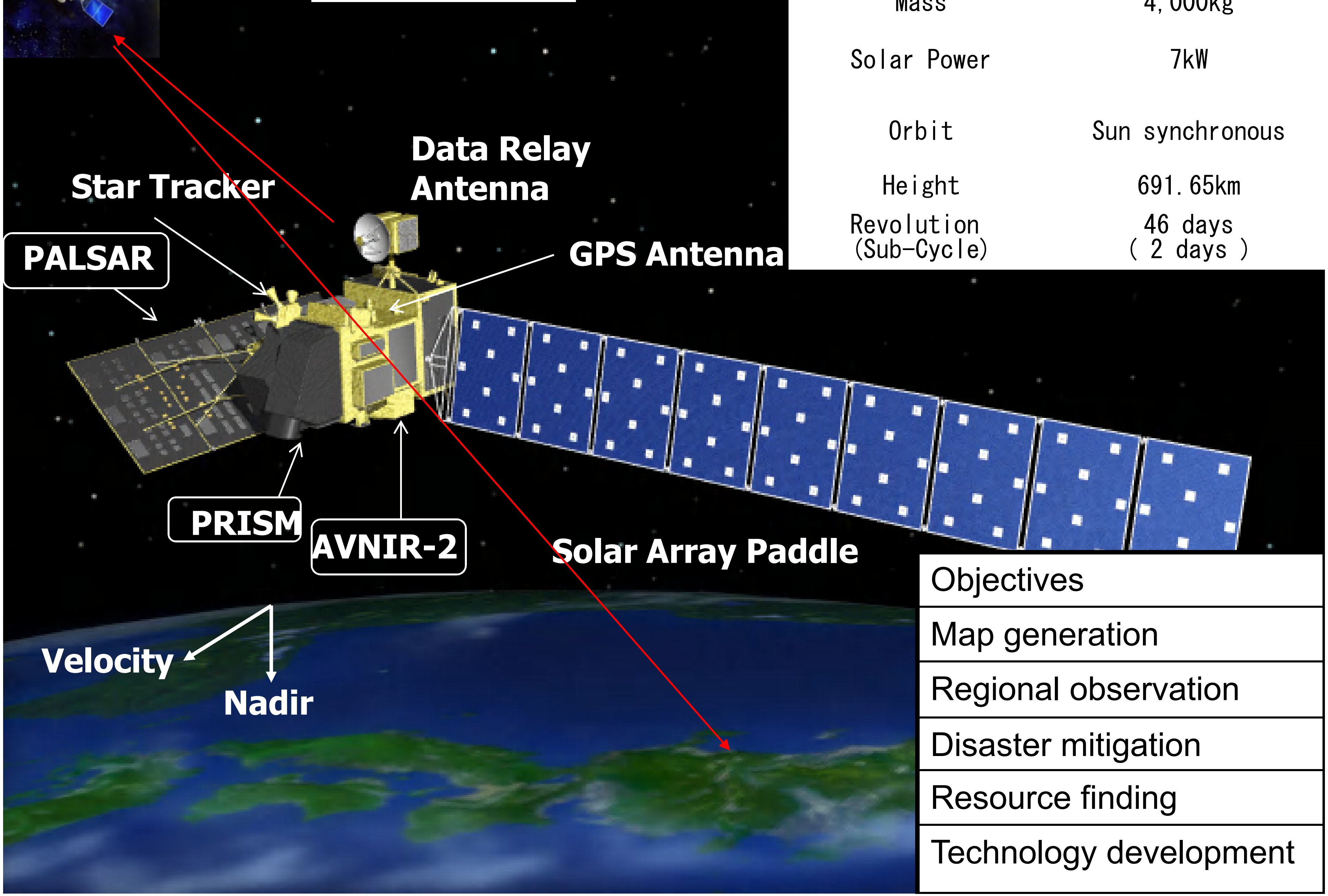

Objectives
Map generation
Regional observation
Disaster mitigation
Resource finding
Technology development

SAR imaging

High resolution imaging
range :FM modulation
Azimuth:Doppler modulation

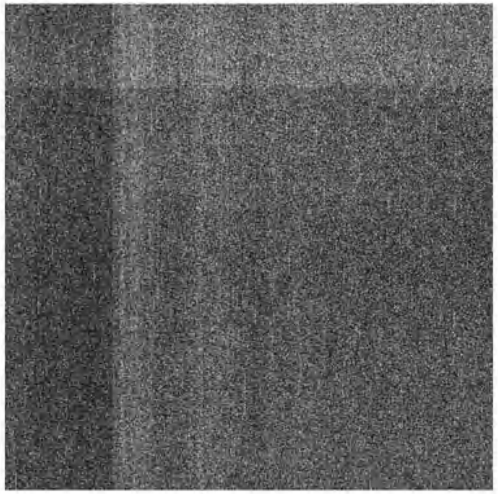

raw data

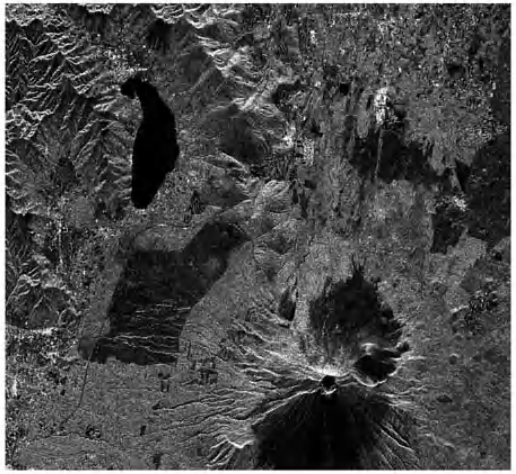

processed

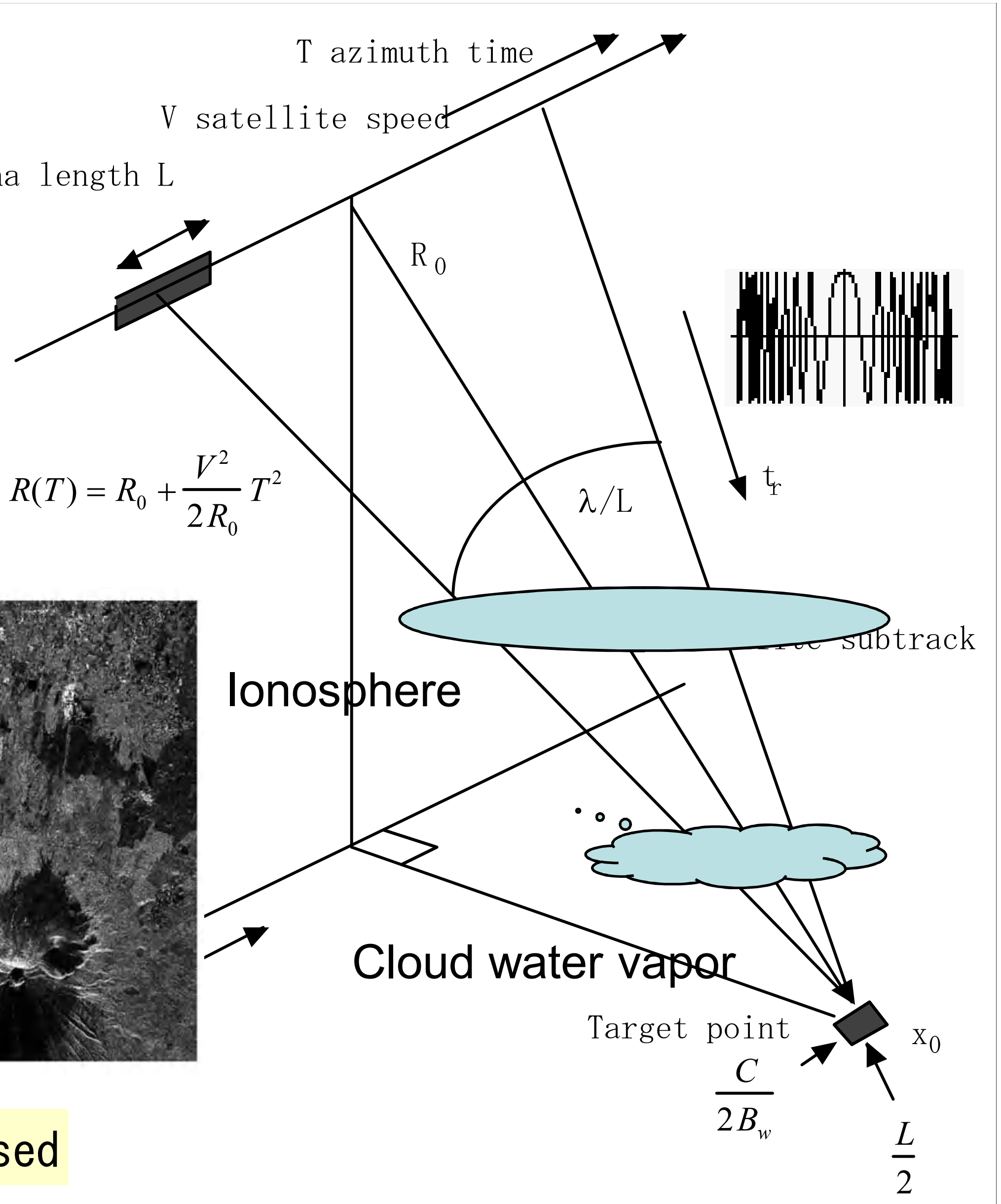

$$S_{ra}(R,x) = A(R,x)\,\mathrm{sin}\,c\left(\frac{2\pi B_w(R-R_0)}{C}\right)\mathrm{sin}\,c\left(2\pi\left(\frac{x-x_0}{L}\right)\right)\exp\left(-\frac{4\pi R_0}{\lambda}j\right)$$

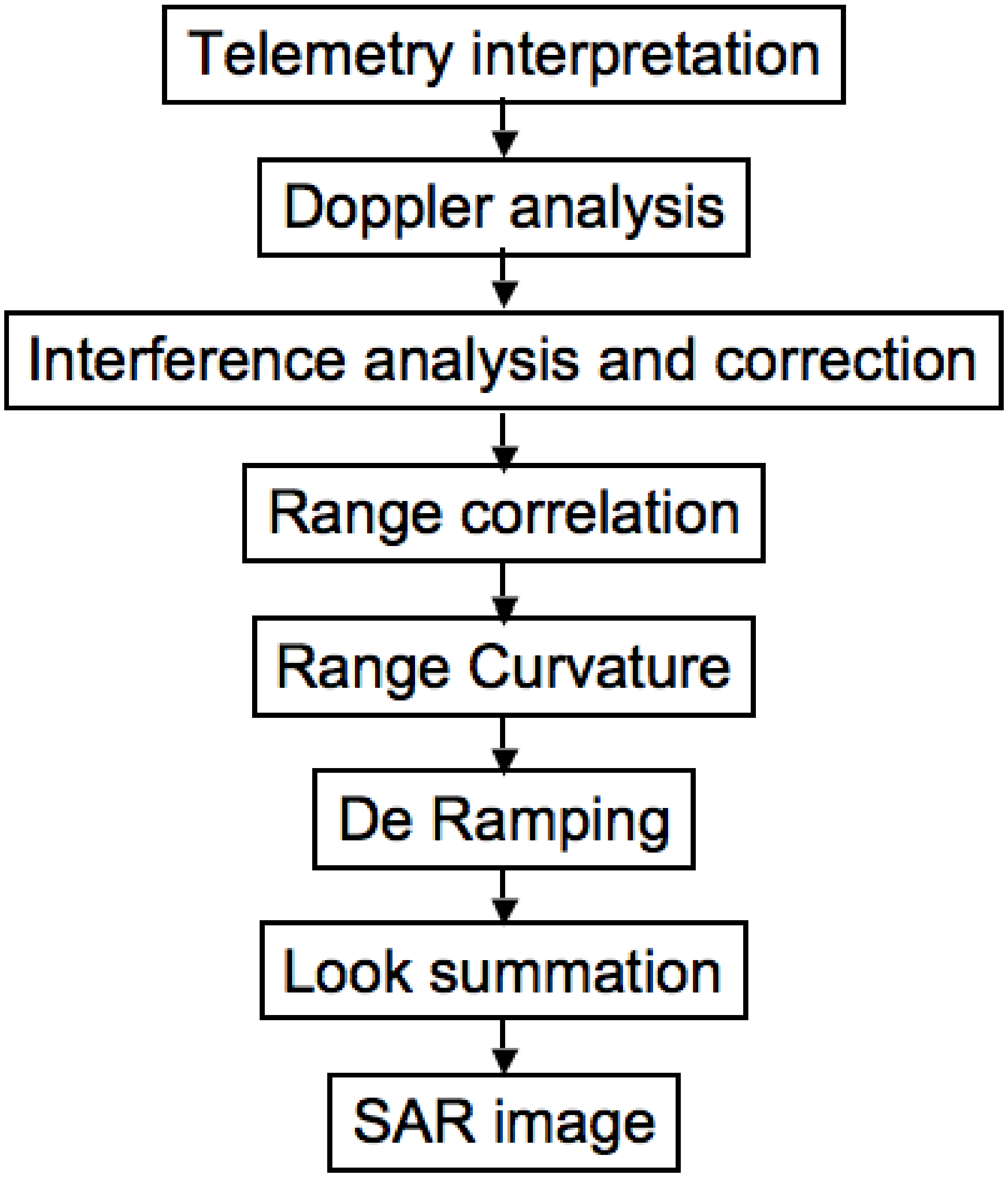
Telemetry interpretation
Doppler analysis
Interference analysis and correction
Range correlation
Range Curvature
De Ramping
Look summation
SAR image

SCANSAR multi looking

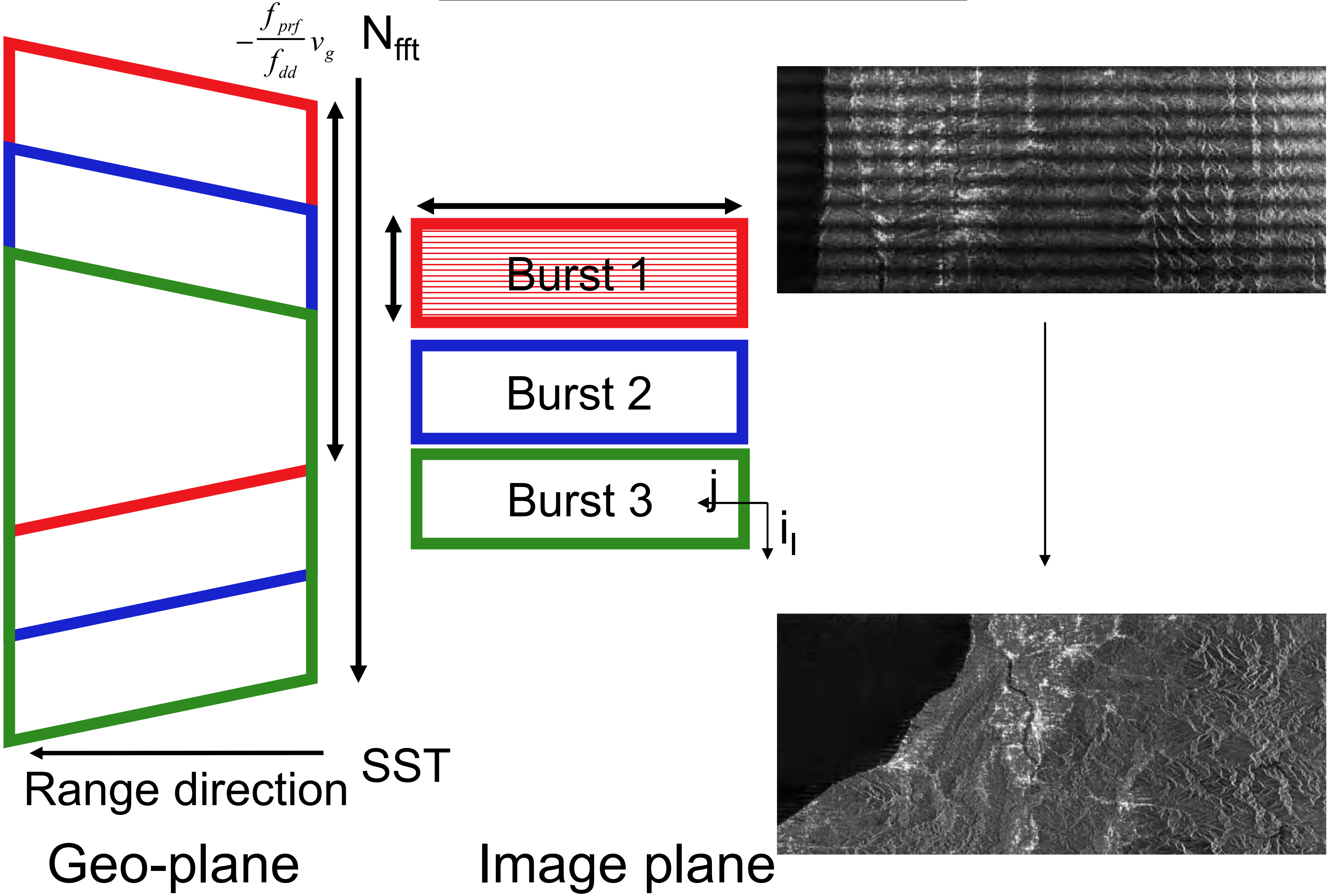

Chirp-z FFT, FFT are used.

SCANSAR幾何精度

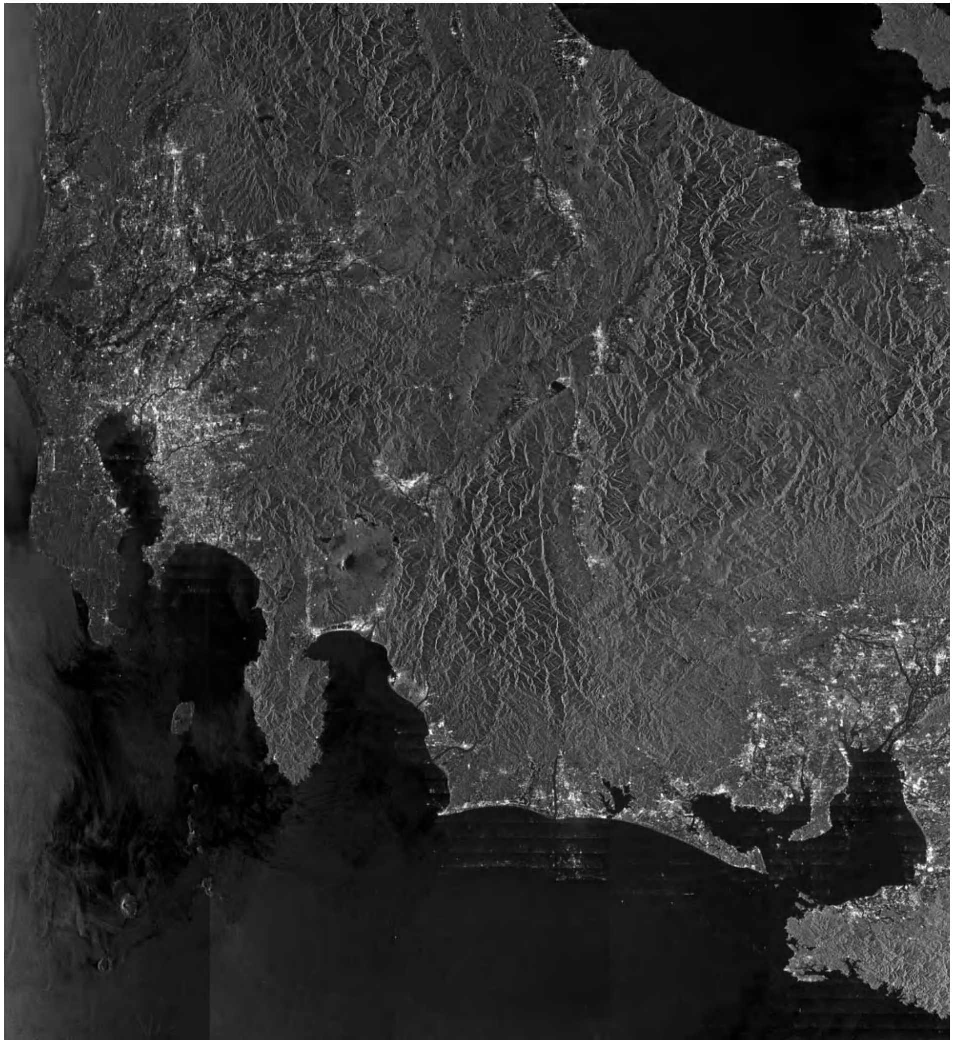

振幅画像（WB1）

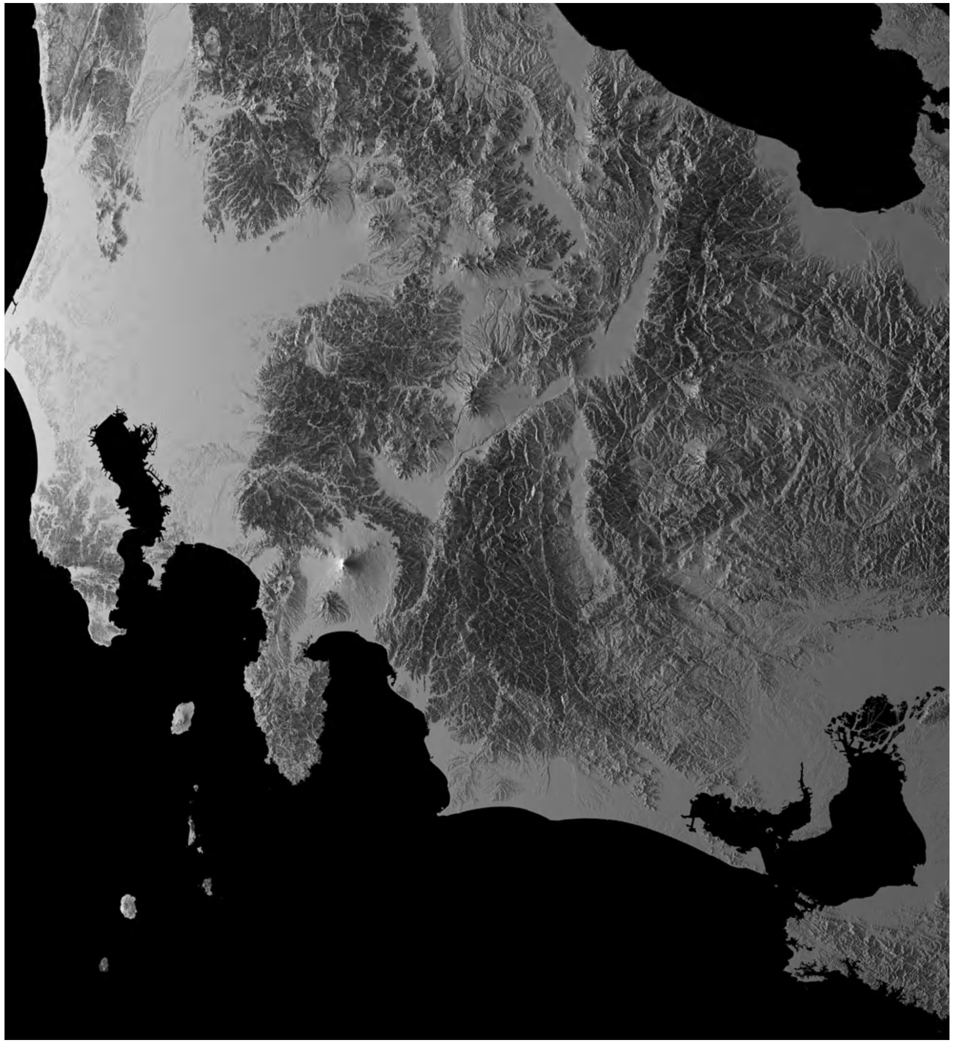

擬似画像（WB1）

幾何学精度
azimuth:　50m
range　：　50m

Sample images of the SCANSAR: Desert

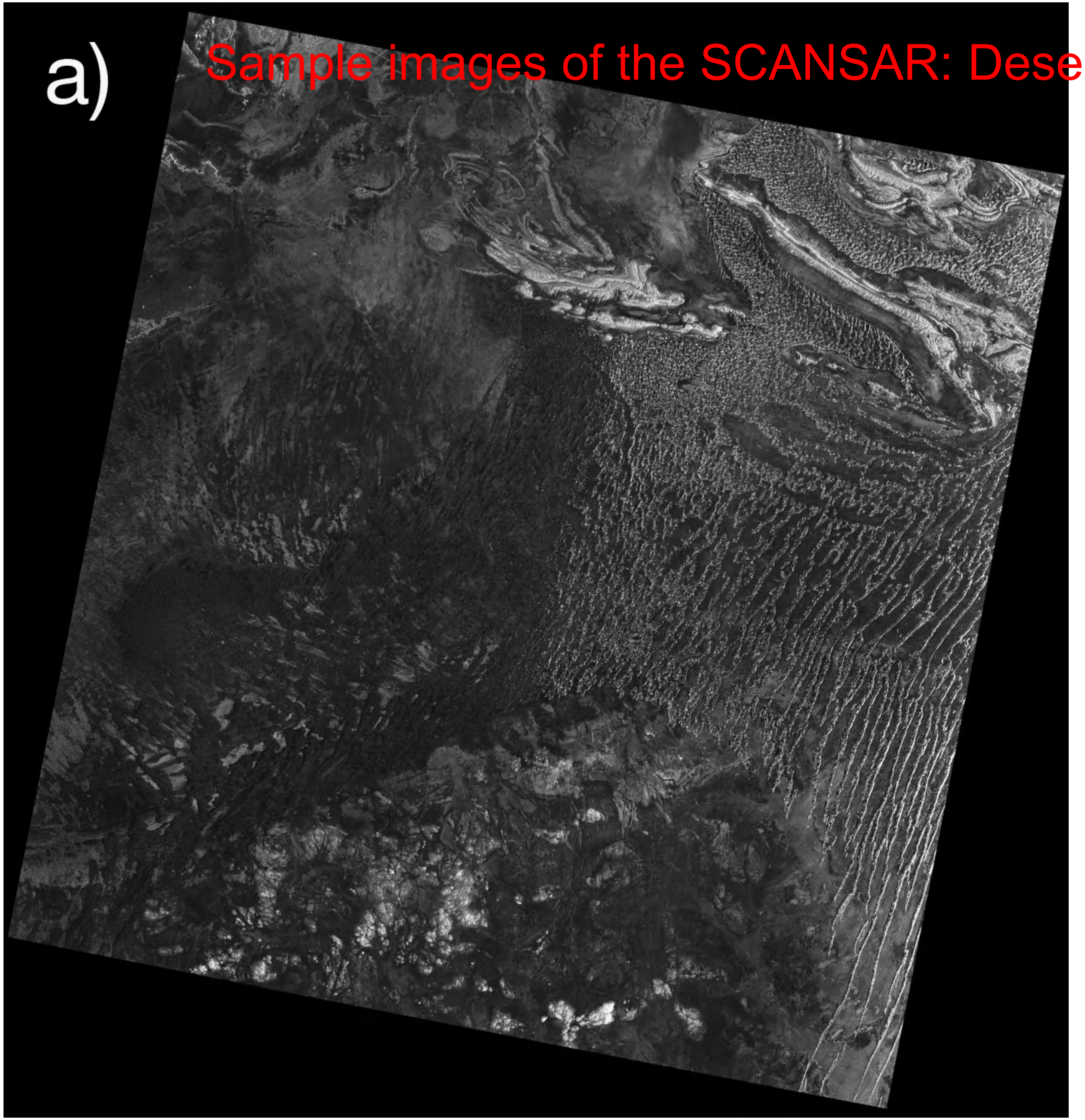

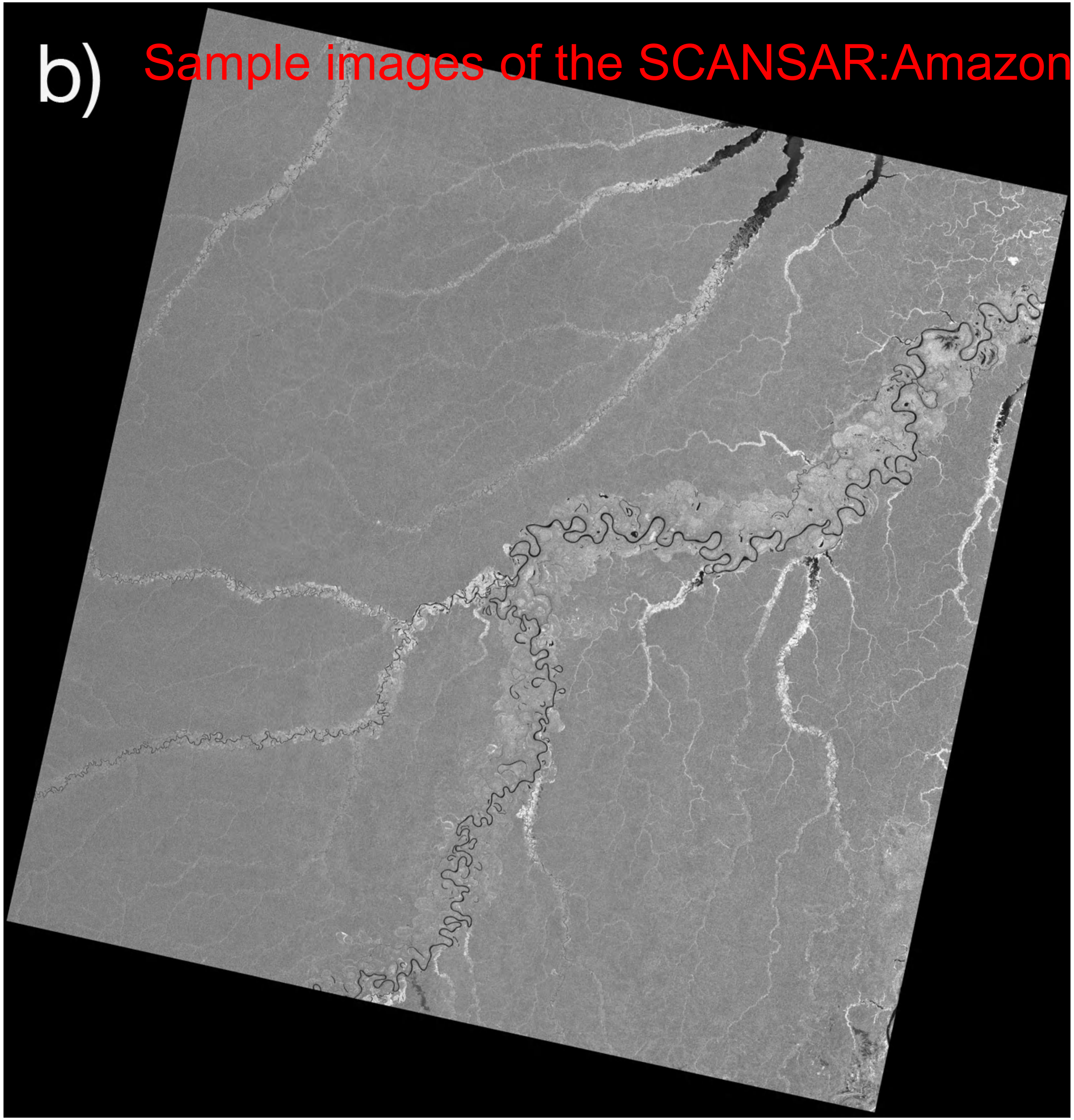
b)
Sample images of the SCANSAR:Amazon

c) Sample images of the SCANSAR:Hokkaido and O

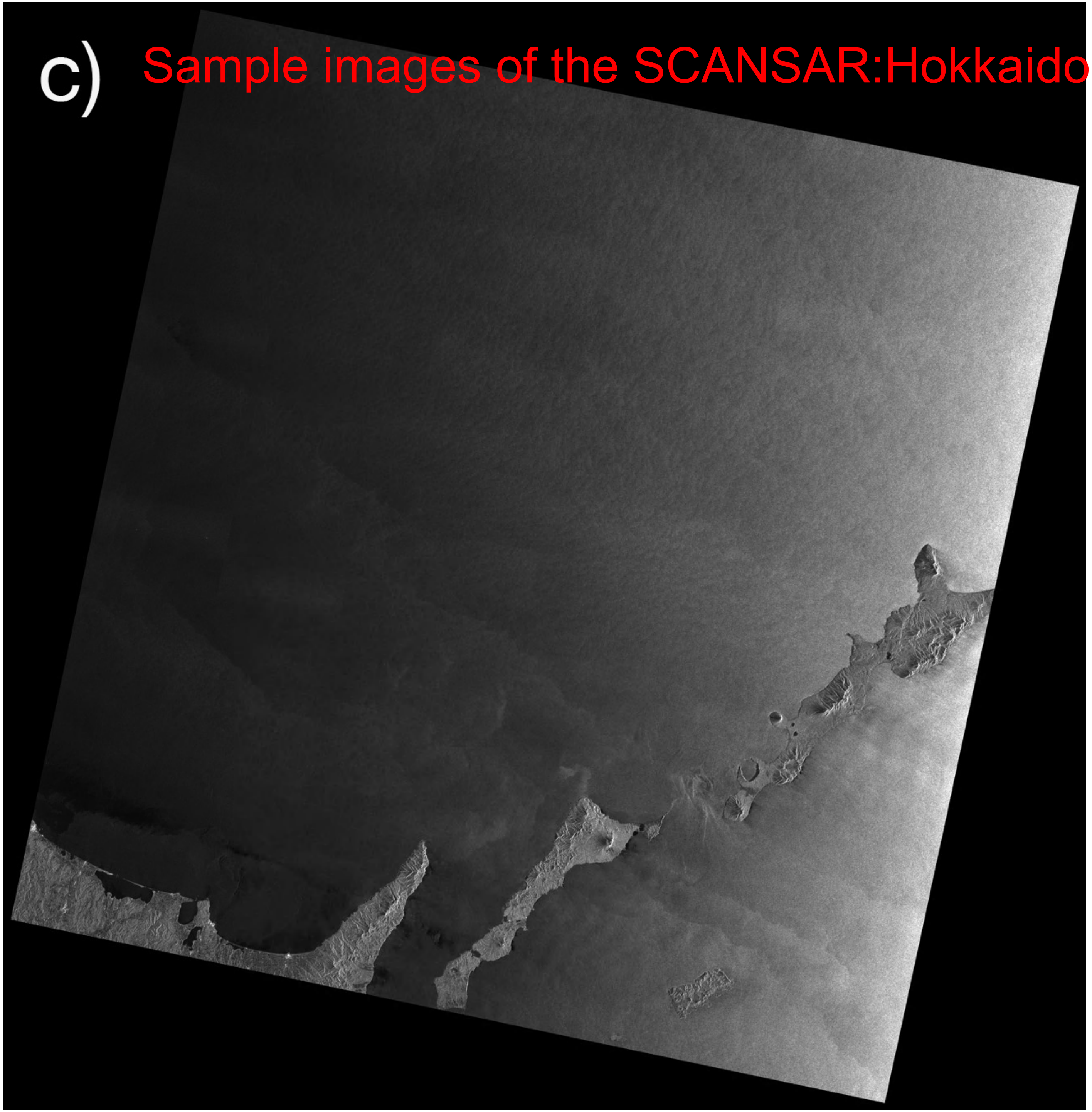

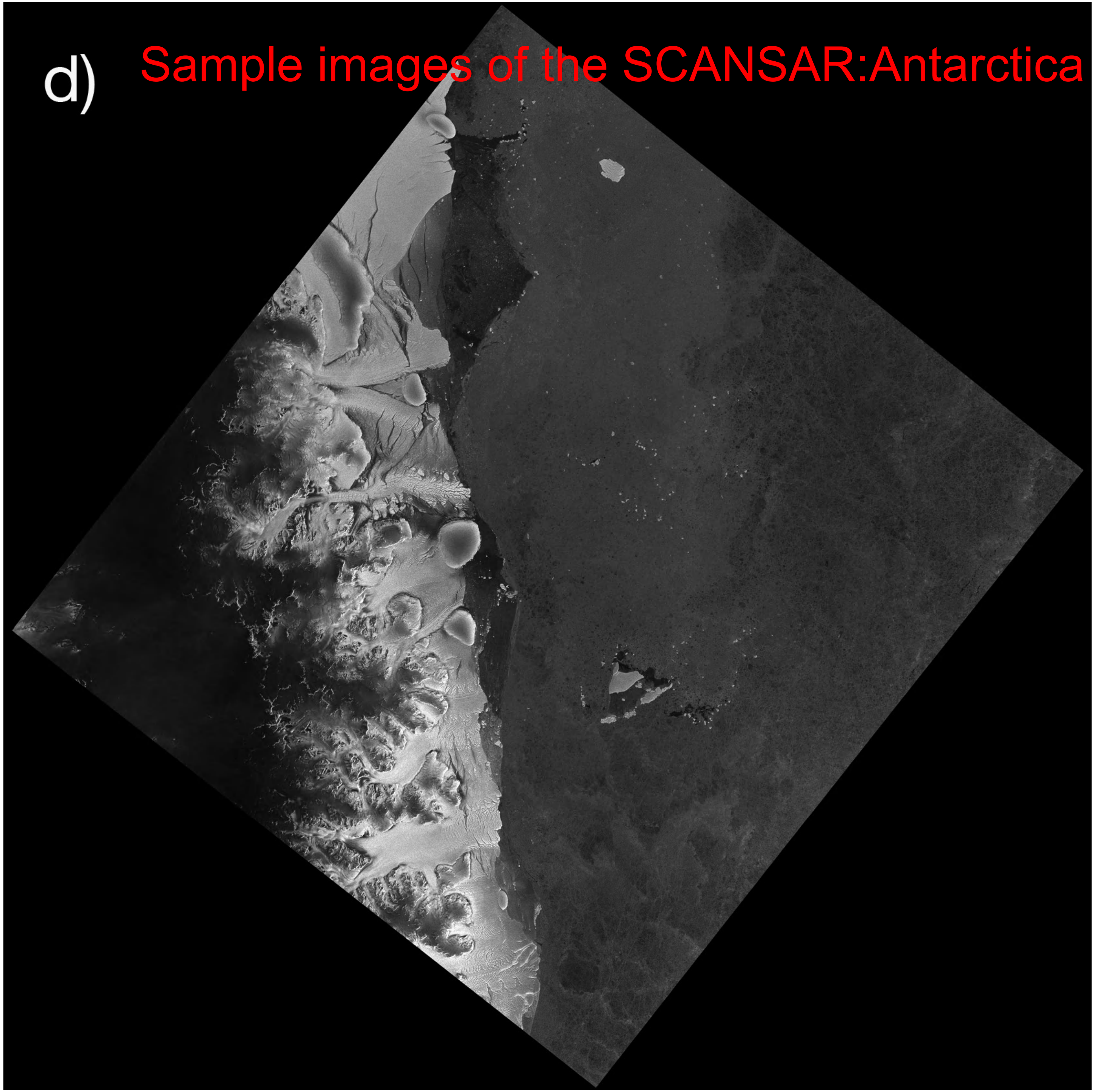
d)
Sample images of the SCANSAR:Antarctica

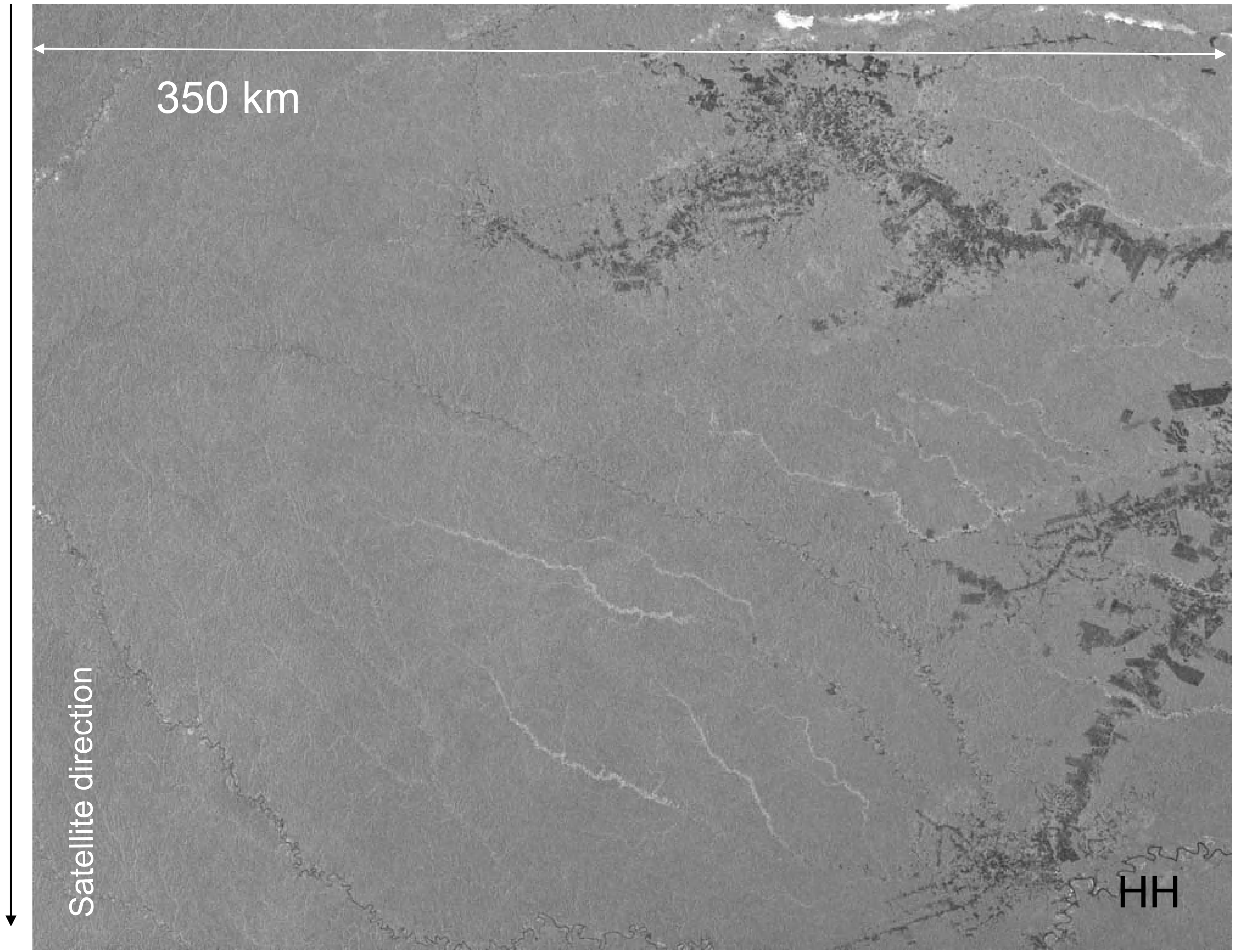

SCANSAR image using the updated antenna pattern and scan-to-scan normalization factors

Transmission power monitor

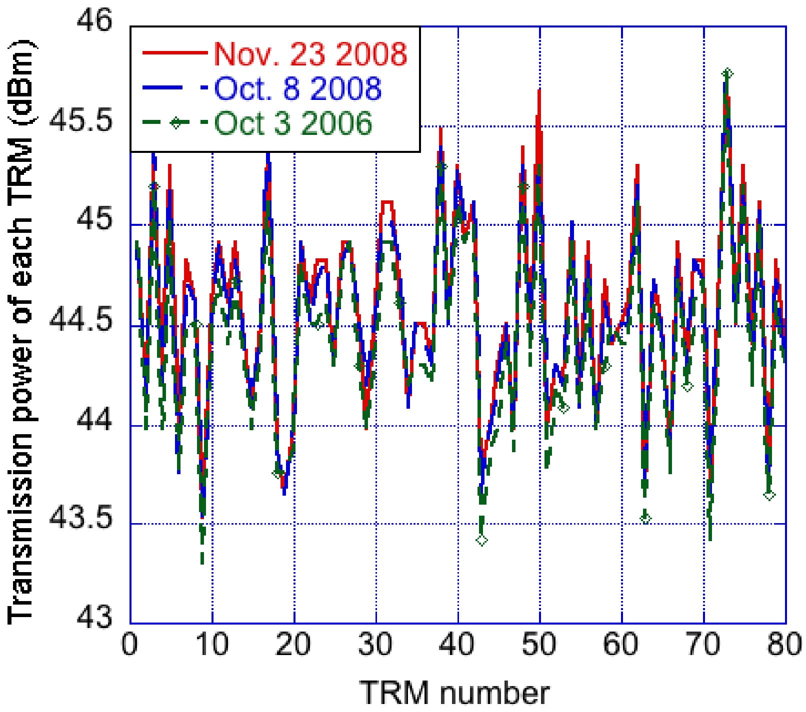

Variation of the Pt
Over 80 TRM

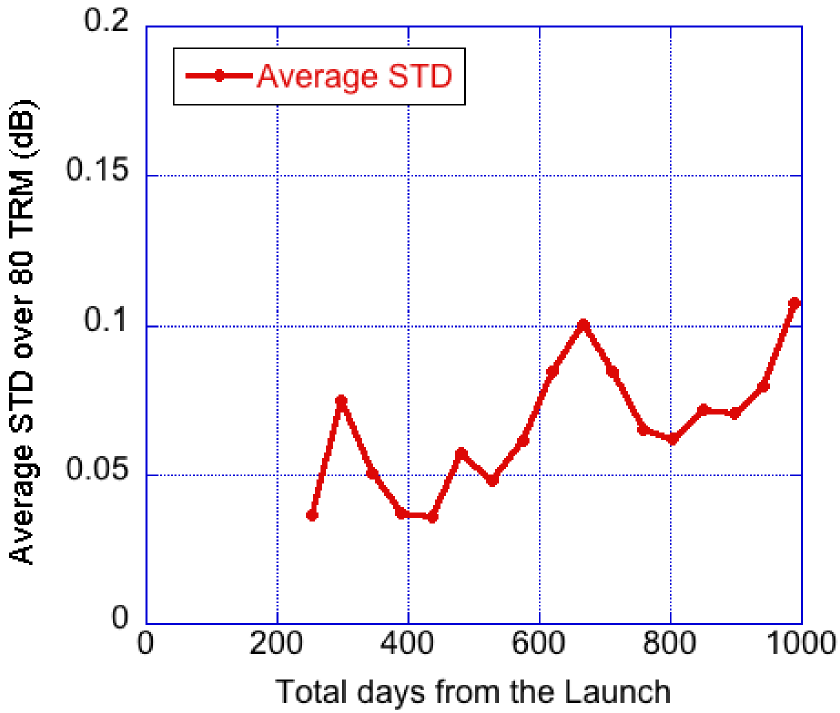

Std Dev. Of Pt

Radiometric/Geometric calibration using the CRs Mode and time dependency over last three years

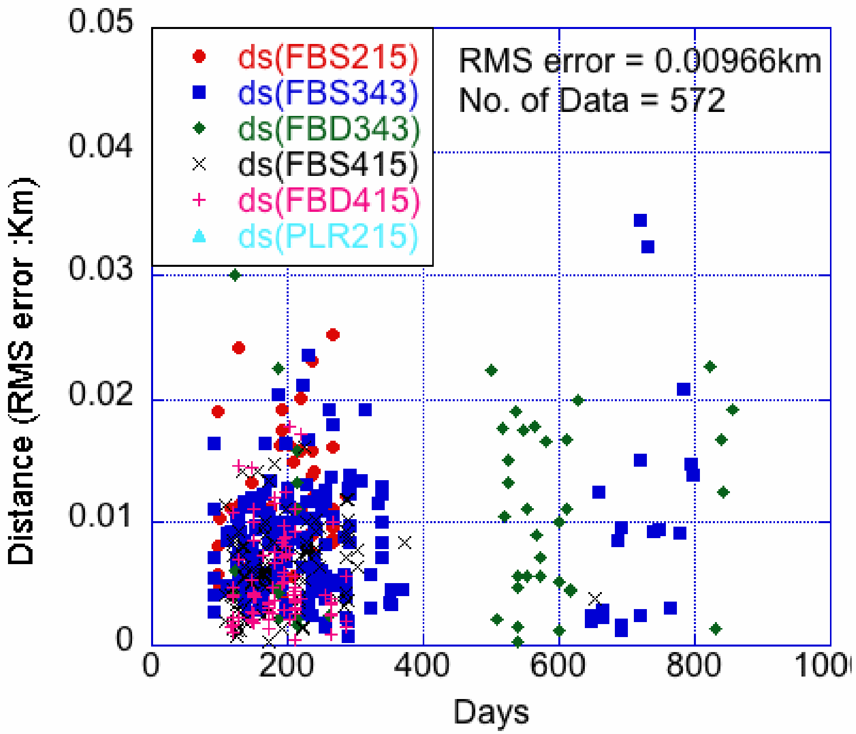

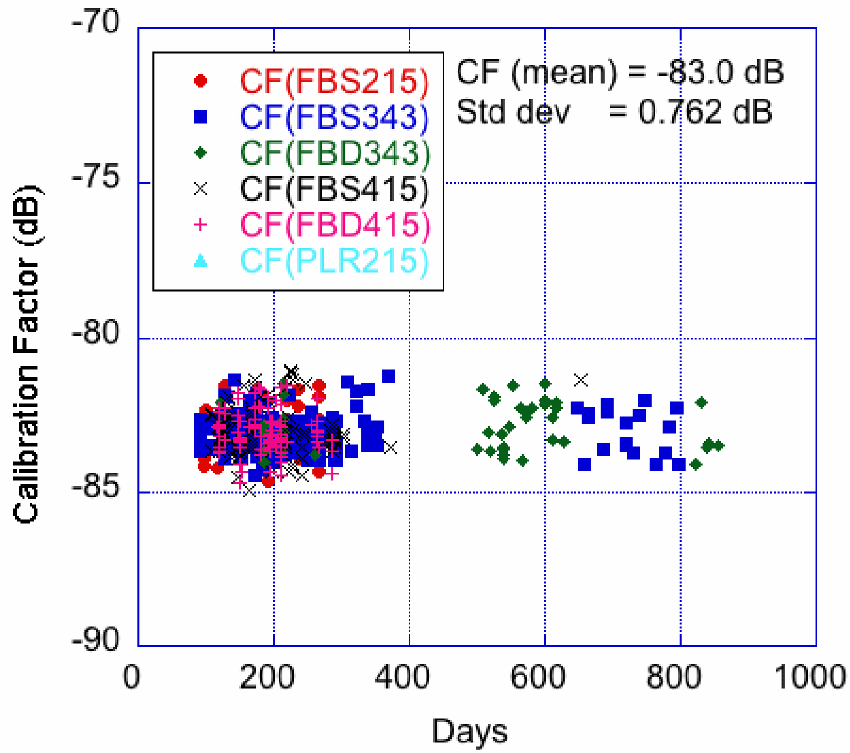

Incidence angle dependence of the gamma naught
Evaluation conducted using the Amazon data

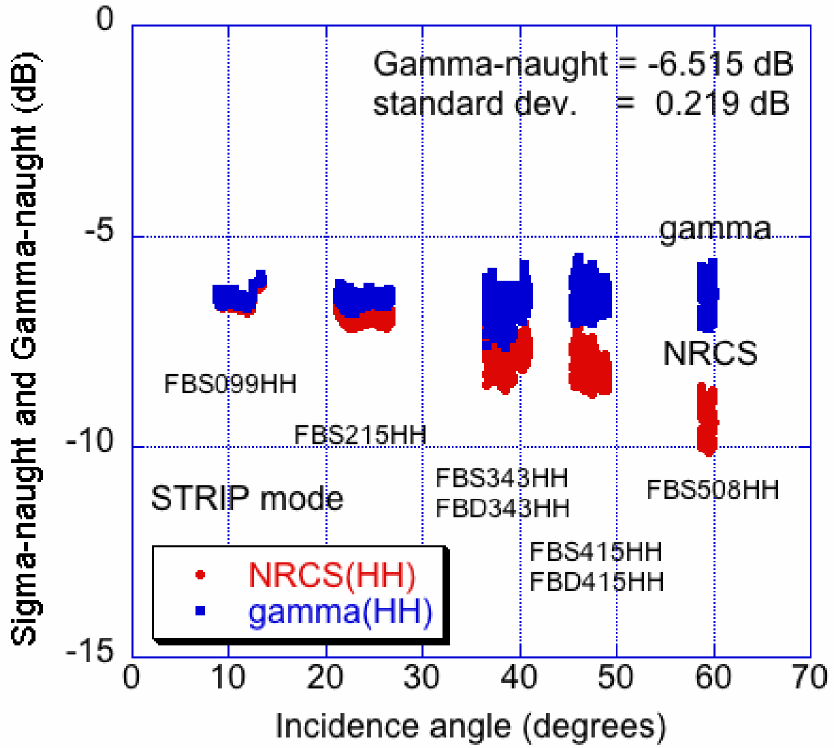

Strip modes

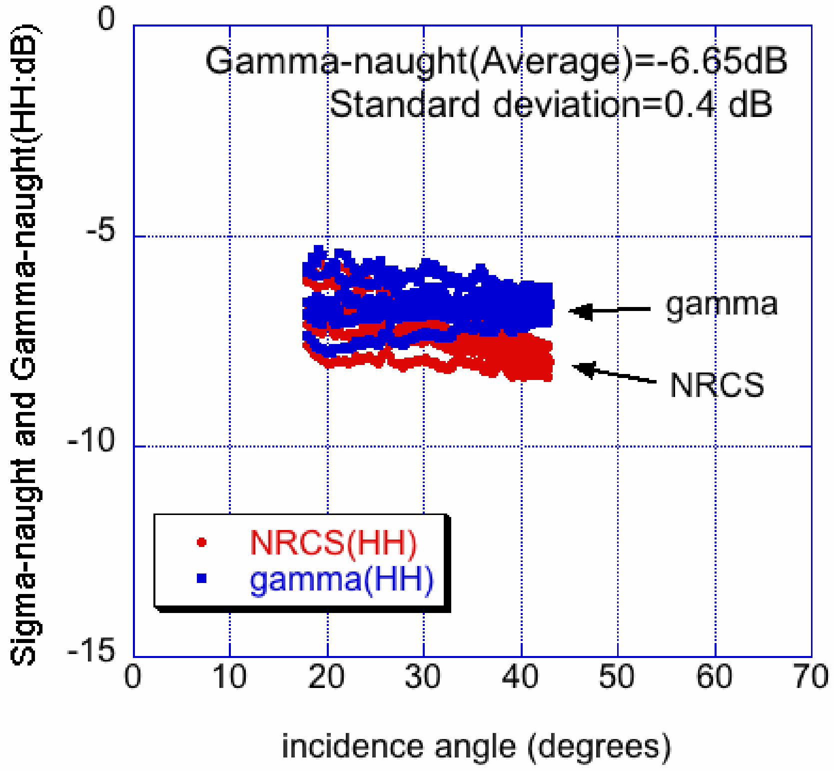

ScanSAR data

Summary of the PALSAR CALVAL results

Table 6 PALSAR Calibration Accuracy

Items	Measured values		No. of Data	Specification
geometric accuracy	9.7m(RMS): STRIP mode		572	100m
	70m(RMS): SCANSAR			
radiometric accuracy	0.219 dB(1 sigma) from Amazon forest 0.76 dB (1 sigma) from CRs 0.17 dB (1sigma: Sweden CRs) -34 dB (Noise equivalent Sigma-zero for HV) -32 dB (as a minimum of FBD-HH) -29 dB (as a minimum of FBS-HH)		 572 16	1.5 dB 1.5 dB 1.5 dB -23 dB
Polarimetric calibration	VV/HH ratio VV/HH phase diff Crosstalk	1.013 (0.062)* 0.612deg(2.66)* -31.7 (4.3)	81	0.2 dB 5 deg. -30 dB
resolution	azimuth range (14MHz) range (28MHz)	4.49 m (0.1) * 9.6m(0.1m) * 4.7m(0.1m)*	572	4.5m 10.7m 5.4m
Side lobe	PSLR in azimuth PSLR in range ISLR	-16.6dB -12.6 dB -8.6 dB	572	-10dB -10dB -8dB
Ambiguity	Azimuth Range	not appeared 23 dB		16dB 16 dB
Transmission power	Sum of 80 TRM	2220W		2000W

Note: A (B)* represents an average value of A and a standard deviation of (B). PSLR is Peak-to-Side-Lobe Ra
ISLR is Integrated Side-Lobe Ratio.

Geometry issue

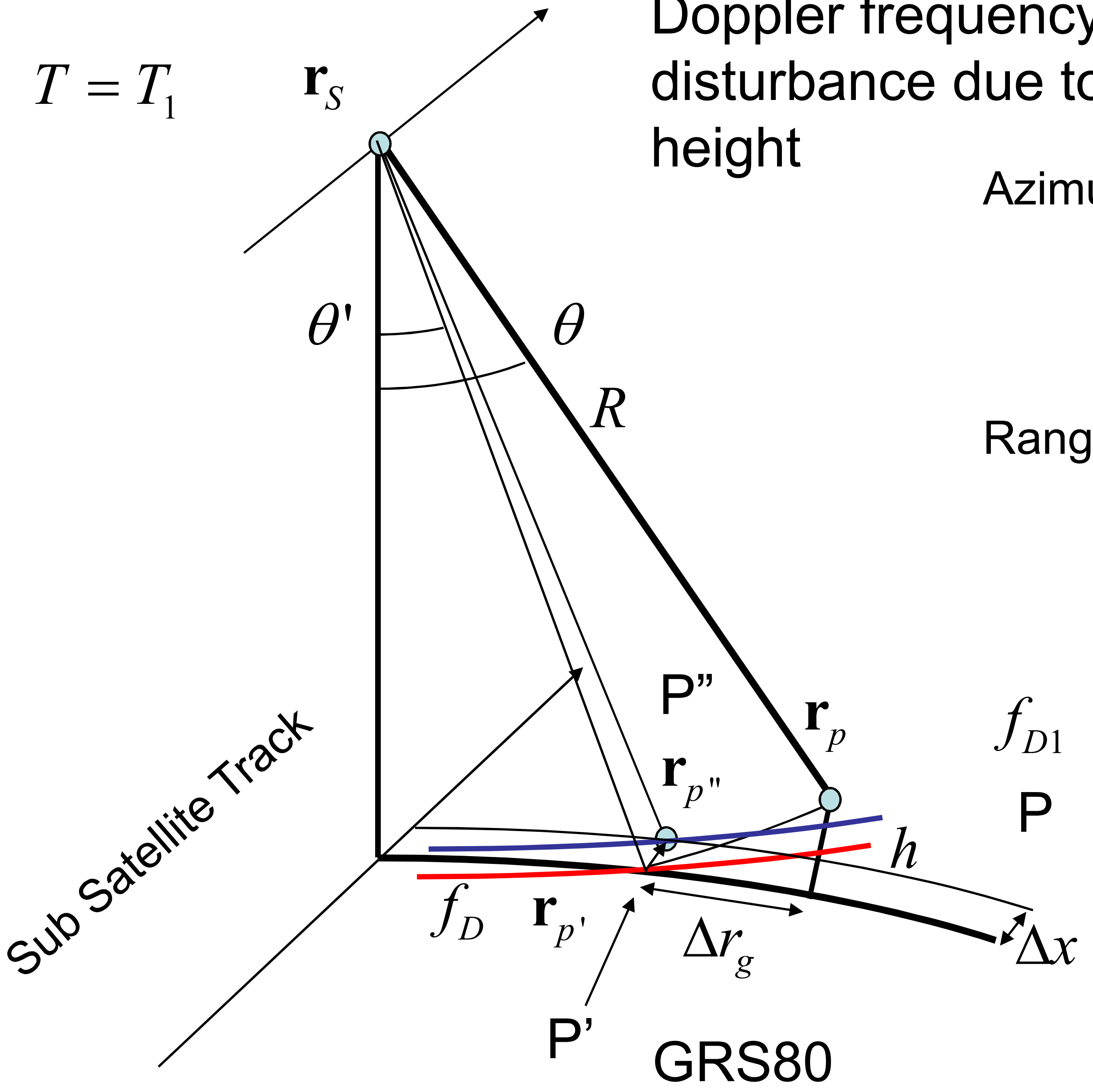

Doppler frequency disturbance due to the height

Azimuth Shift

$$\Delta x = -\frac{\Delta f_D}{f_{DD}} v_g$$

Range Shift (1st order)

$$\Delta r_g \cong \frac{h}{\tan \theta_{inci}}$$

Determination of the scattering point

Iterations/approximation

$$f_{d1} = \frac{2}{\lambda}\left(\mathbf{u}_s - \omega \times \mathbf{r}_p\right)\frac{\left(\mathbf{r}_p - \mathbf{r}_s\right)}{\left|\mathbf{r}_p - \mathbf{r}_s\right|}$$

$$r = \left|\mathbf{r}_p - \mathbf{r}_s\right|$$

$$\frac{x_p^2}{R_a^2} + \frac{y_p^2}{R_a^2} + \frac{z_p^2}{R_b^2} = 1$$

$$R_a = \bar{R}_a + \left\{h(\varphi,\lambda) + h_{geoid}(\varphi,\lambda)\right\}\sqrt{1 - e^2 \sin^2 \varphi}$$

$$R_b = R_a\sqrt{1 - e^2 \sin^2 \varphi}$$

$$e^2 = \frac{R_a^2 - R_b^2}{R_a^2}$$

h :Height from the geoid

h_{geoid} :Geoid

Features
Solutions are accurate. However, layover and shadowing areas are suffered from the non-solution problems.

Geometric Evaluation Result

Geo error (ortho) > Geo error (slant)

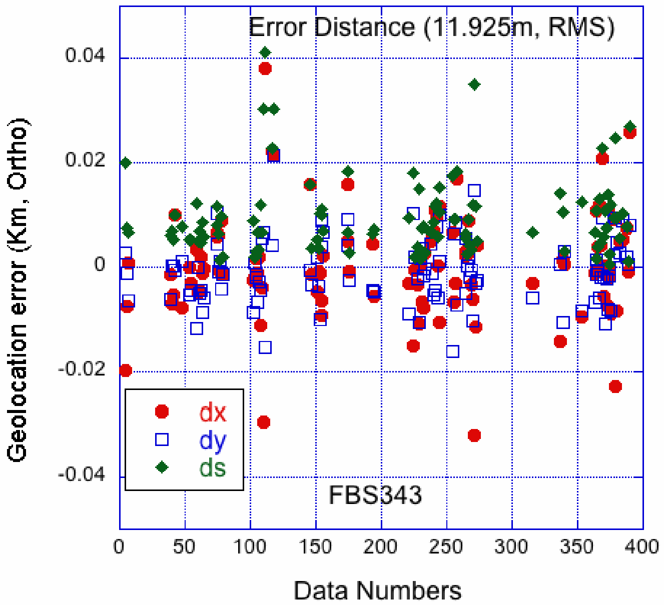

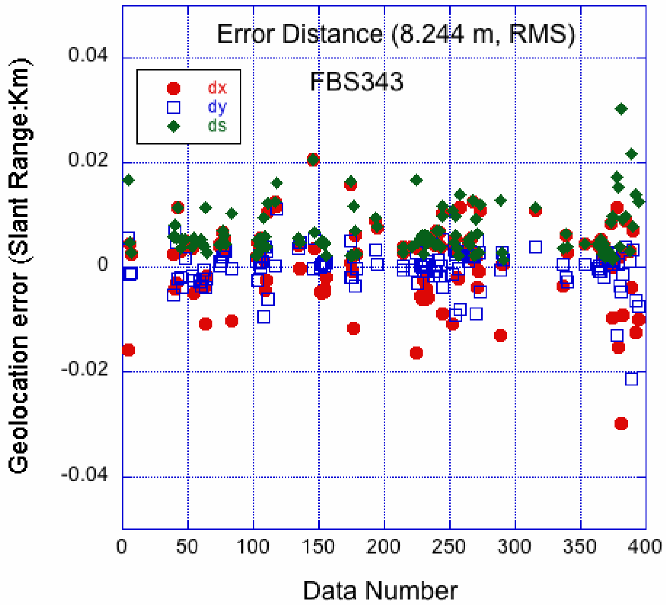

TABLE IV Geolocation Accuracy Measurement for the Ortho-rectification Image and Slant Range Image

Off-nadir Angle (^{o})	Geolocation Error (ortho: m)	Geolocation Error (Slant: m)
21.5	17.383 (7.211, 21)	13.19 (5.267, 28)
34.3	11.925 (7.266, 104)	8.244 (4.716, 124)
41.5	9.488 (5.127, 50)	7.286 (4.017, 56)
Total Value in RMSE	12.103 (6.718, 175)	8.885 (4.619, 208)

Note: Values in each element are RMSE defined Eq. (28) (standard deviation, number of samples)

G_err_ortho ~12.10m (RMSE)

Position estimation of the ortho-rectified image

TABLE V Comparison of the Ortho-rectified Geometric Accuracy

No.	Latitude	Longitude	Height (m)	Δx (m)	Δy (m)	Δs (m)
Ascending	N35□20Õ13.00́	E138□43Õ57.03́	2410.625	0.253	3.092	3.102
Truth (asc)	N35□20Õ12.97́	E138□43Õ57.02(	2412.449			
Descending	N35□20Õ13.09(	E138□43Õ55.90(	2410.000	3.040	3.711	4.797
Truth (desc)	N35□20Õ12.97́	E138□43Õ55.78(	2412.449			

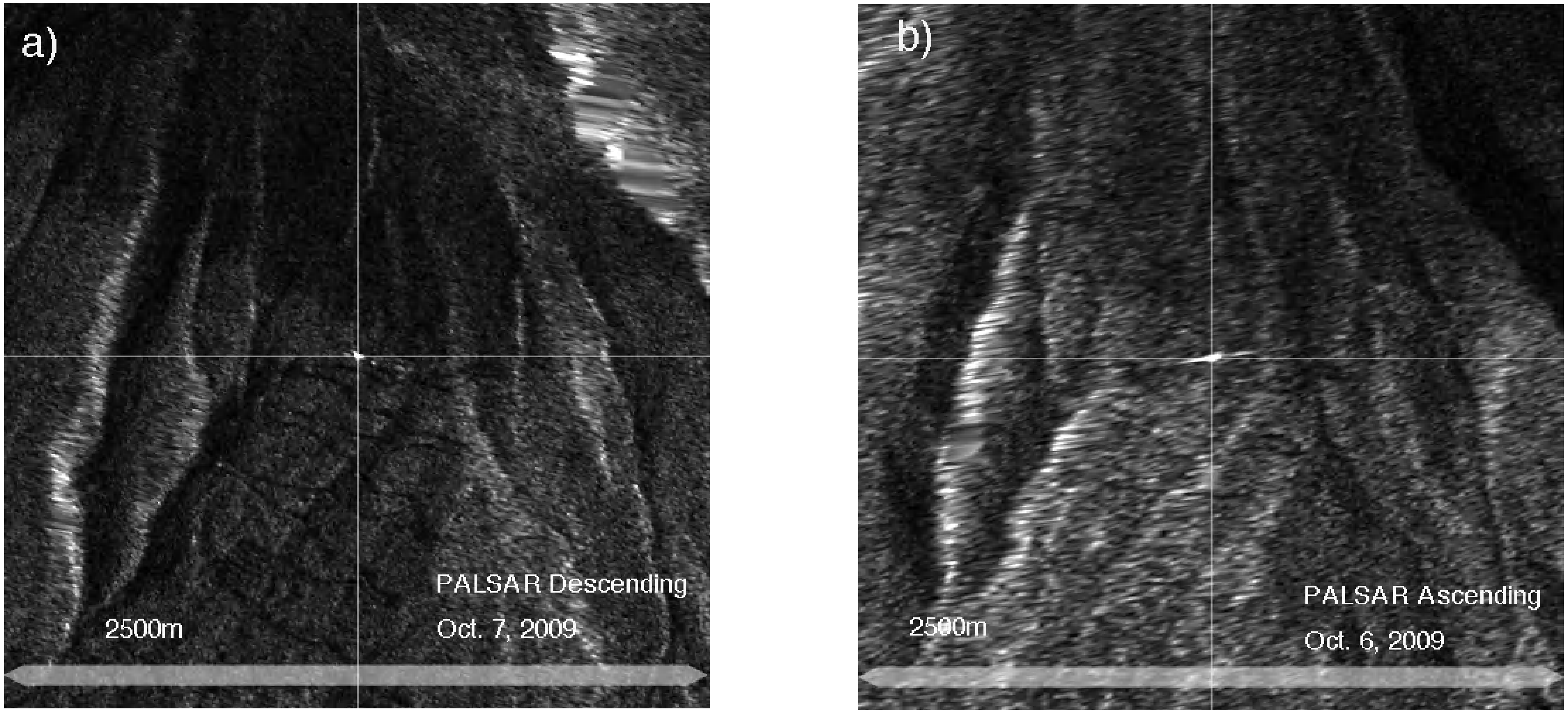

Slope correction

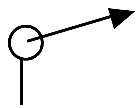

Radiometry issue

- Sigma-naught
- Gamma-naught
- Beta-naught

$$\sigma^0 = \lim_{R\to\infty} \frac{4\pi R^2 \left\langle E_s E_s^* \right\rangle}{A \left\langle E_i E_i^* \right\rangle}$$

$$= \frac{\sigma}{A}$$

$$\gamma^0 = \frac{\sigma^0}{\cos\theta}$$

$$\beta^0 = \frac{\sigma^0}{\sin\theta}$$

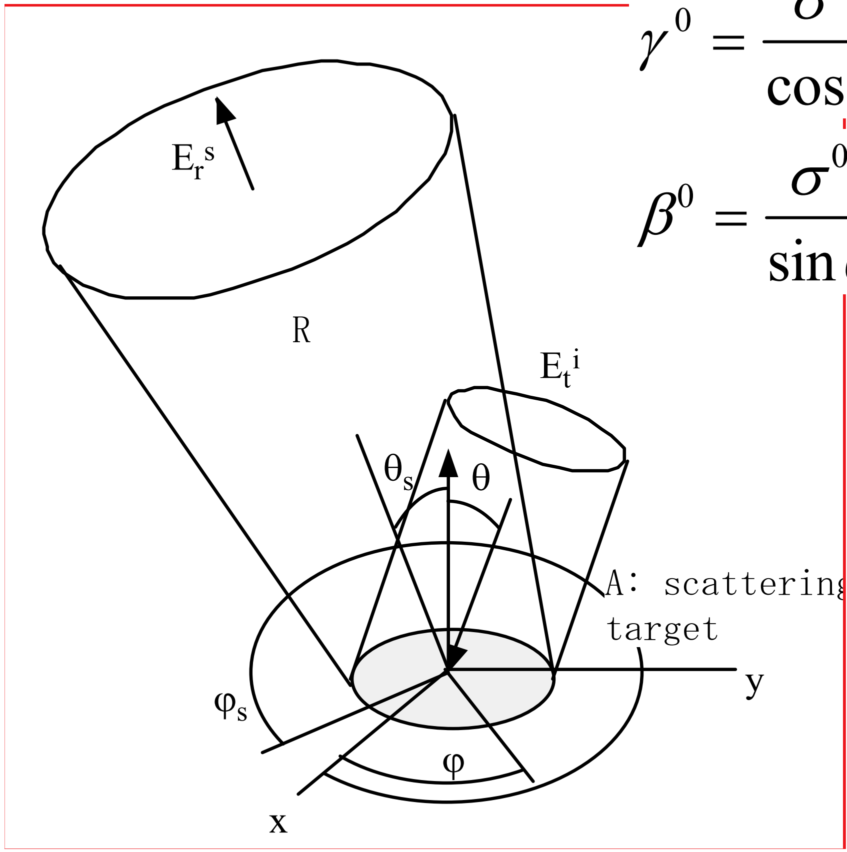

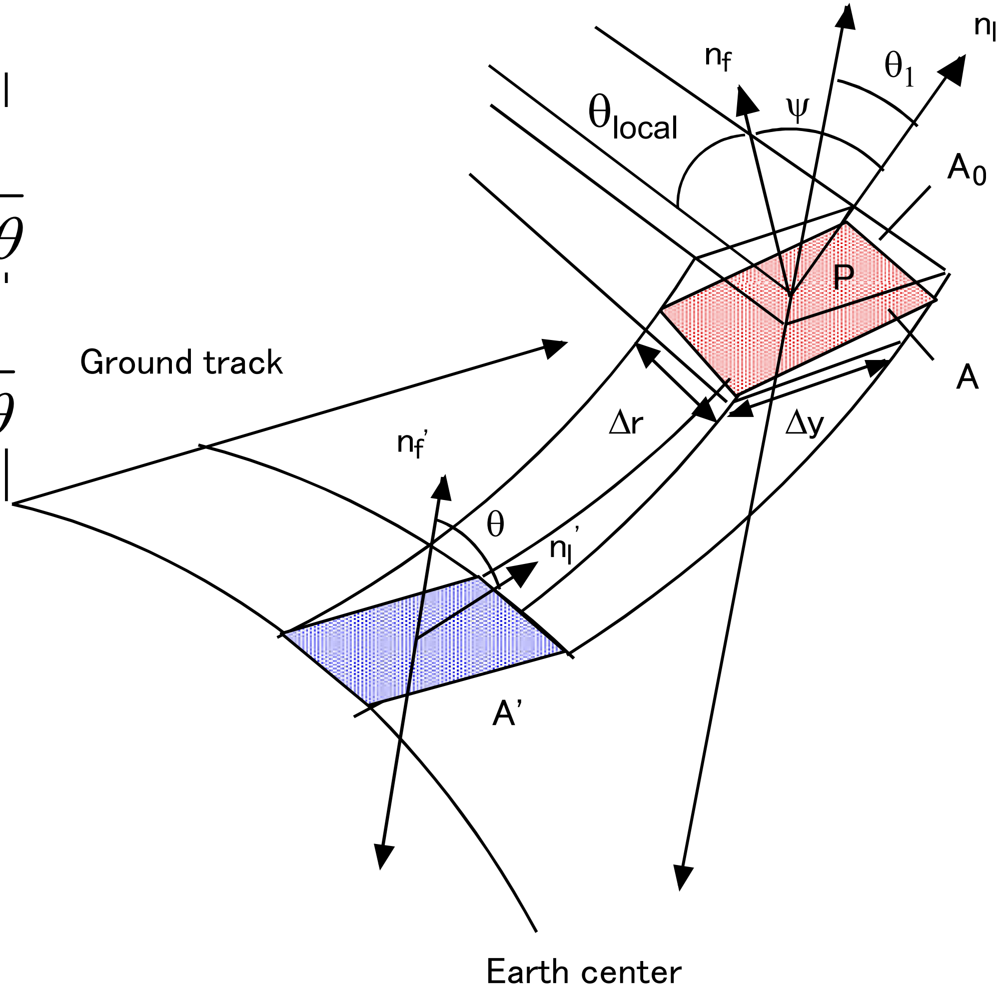

Radiometry:Slope corrections on σ^0 and γ^0

$$\tilde{\sigma}^0 = \sigma^0 \frac{\cos\psi}{\sin\theta} \frac{1}{LIAC}$$

$$\theta_l = \cos^{-1}\left\{ \frac{(\mathbf{r}_s - \mathbf{r}_p)}{|\mathbf{r}_s - \mathbf{r}_p|} \cdot \mathbf{n}_l \right\}$$

$$\mathbf{n}_l = \frac{1}{\sqrt{h_x^2 + h_y^2 + 1}} \begin{pmatrix} h_x & h_y & 1 \end{pmatrix}^t$$

$$\cos\psi = \mathbf{n}_f \cdot \mathbf{n}_l = \frac{\sin\theta_l - \cos\theta_l \cdot h_x}{\sqrt{h_x^2 + h_y^2 + 1}}$$

$$LIAC \sim 10^{d\theta_l}$$

$$\gamma^0 \equiv \frac{\sigma^0}{\cos\theta_{local}} \frac{\cos\psi}{\sin\theta_{inci}}$$

$$\theta_{local} = \cos^{-1}\left\{ \frac{(\mathbf{r}_s - \mathbf{r}_p)}{|\mathbf{r}_s - \mathbf{r}_p|} \cdot \mathbf{n}_l \right\}$$

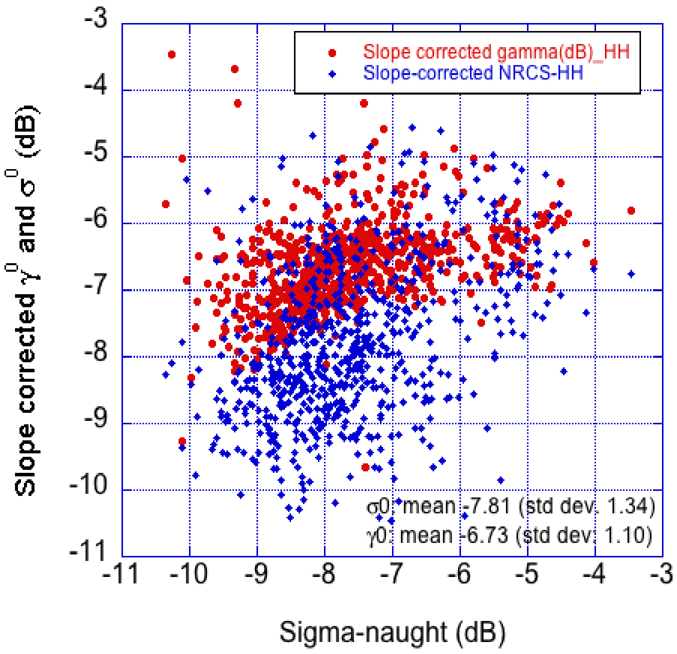

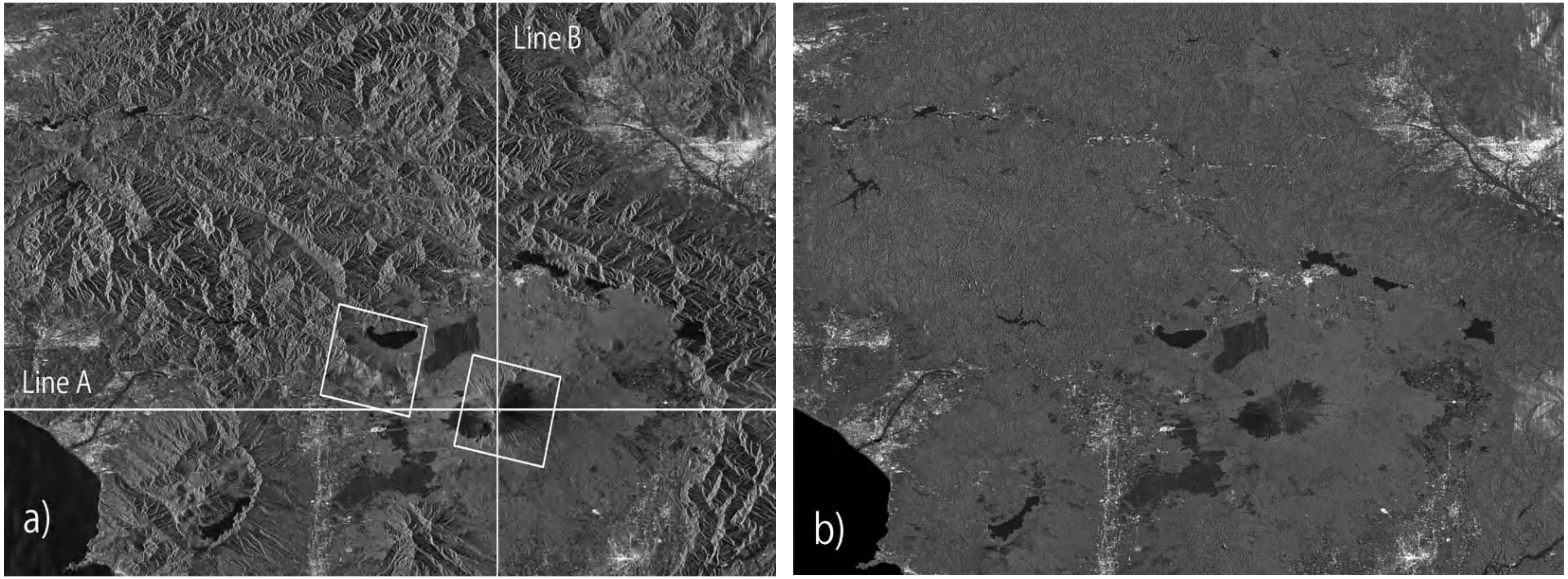
Line B
Line A
a)
b)

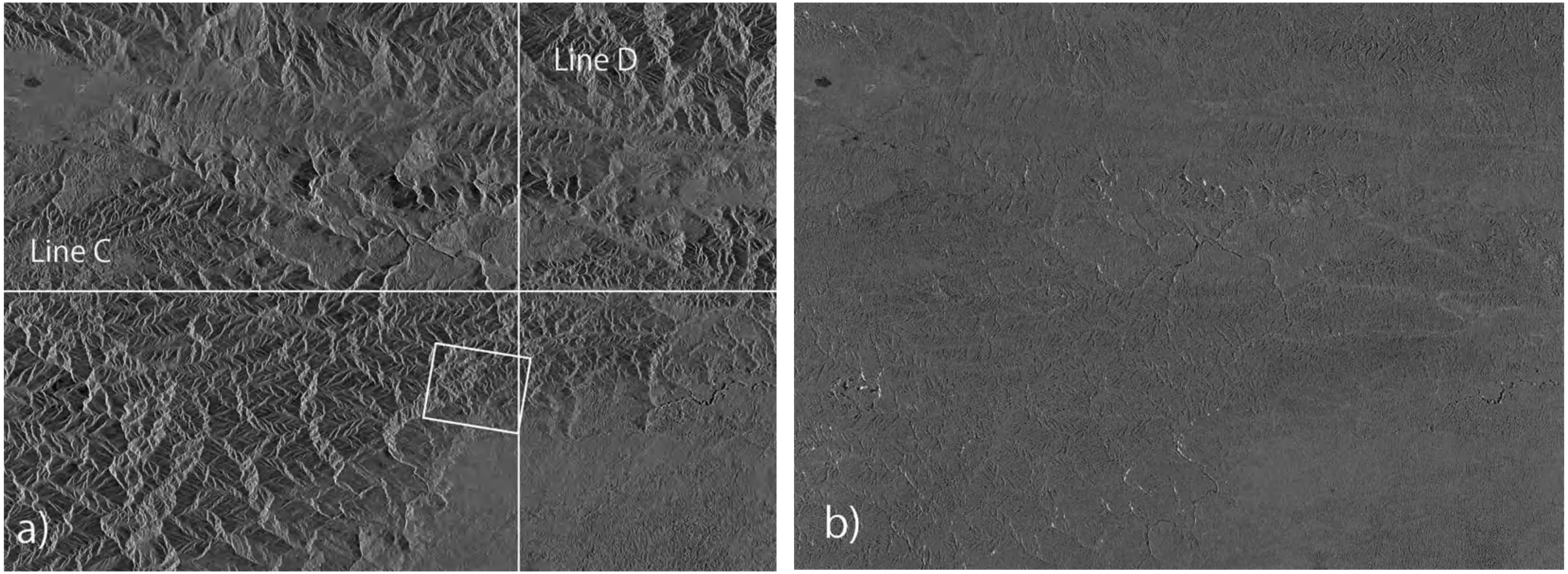
Line D
Line C
a)
b)

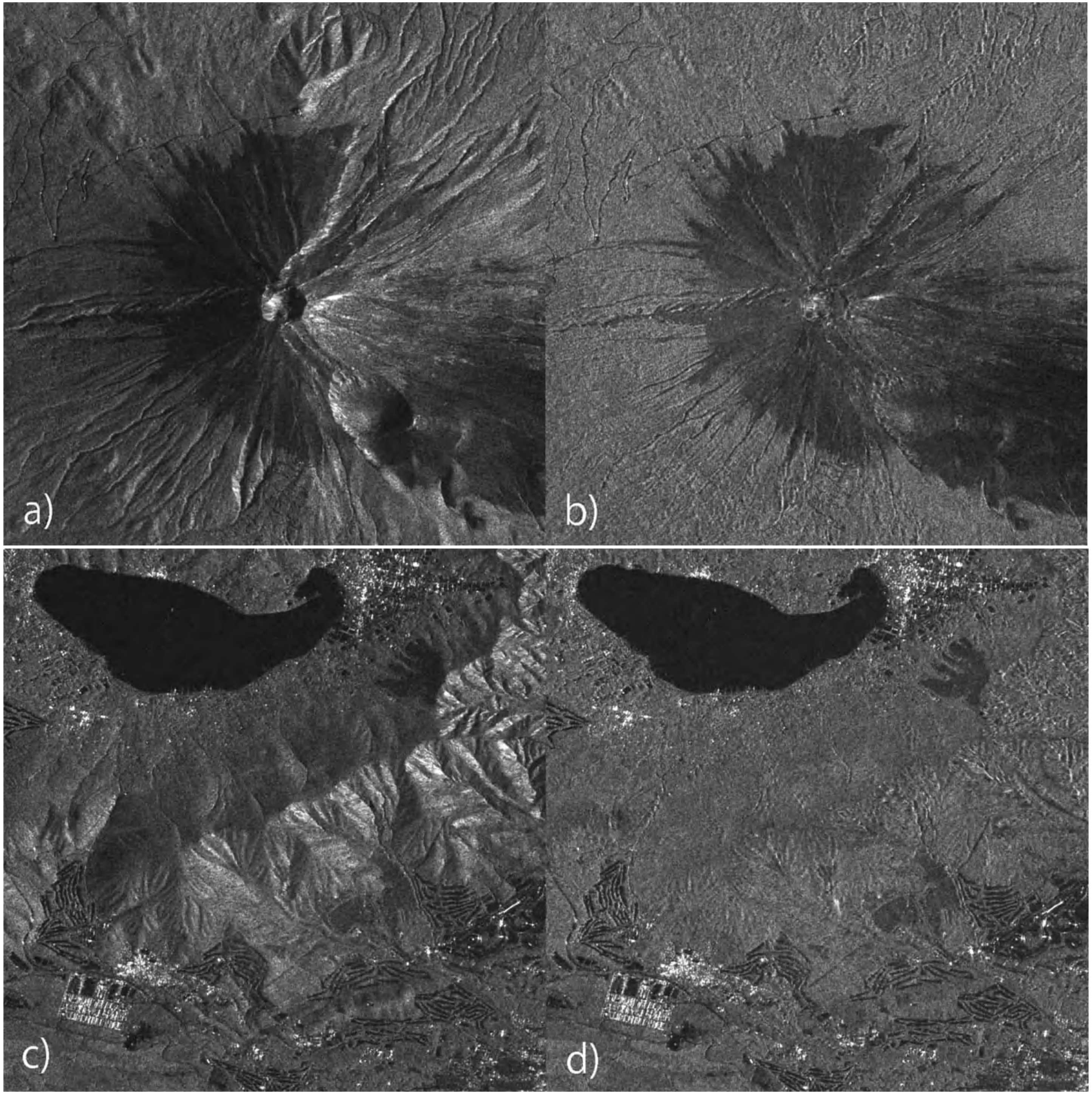
a)
b)
c)
d)

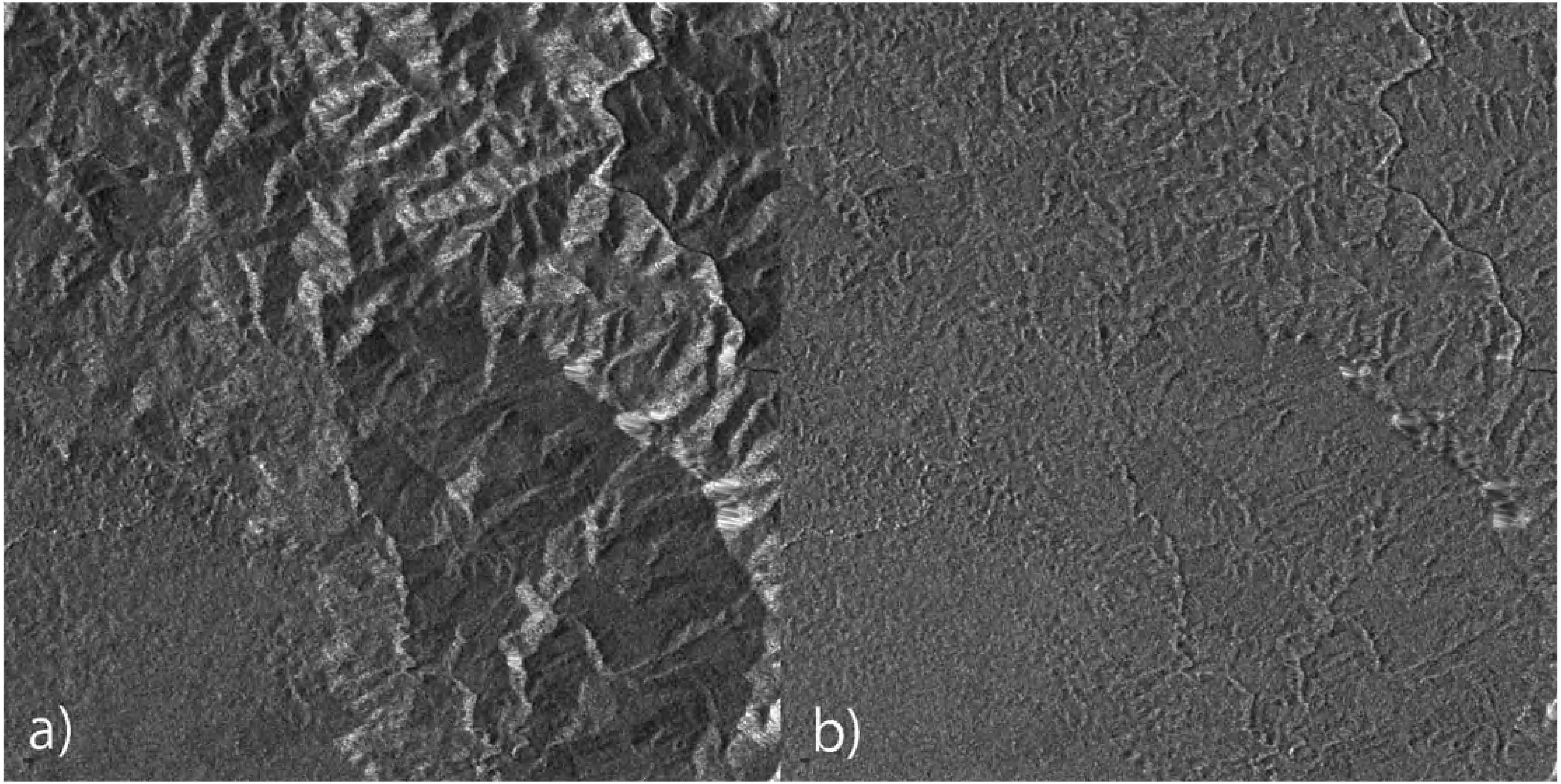

a)
b)

7. Mosaicking and SAR Strip Processing

Advantages:

Global researches

Temporal variation

Reduce the number of images : 86400 -> 1000

Requirements

Geometric and radiometric collocations

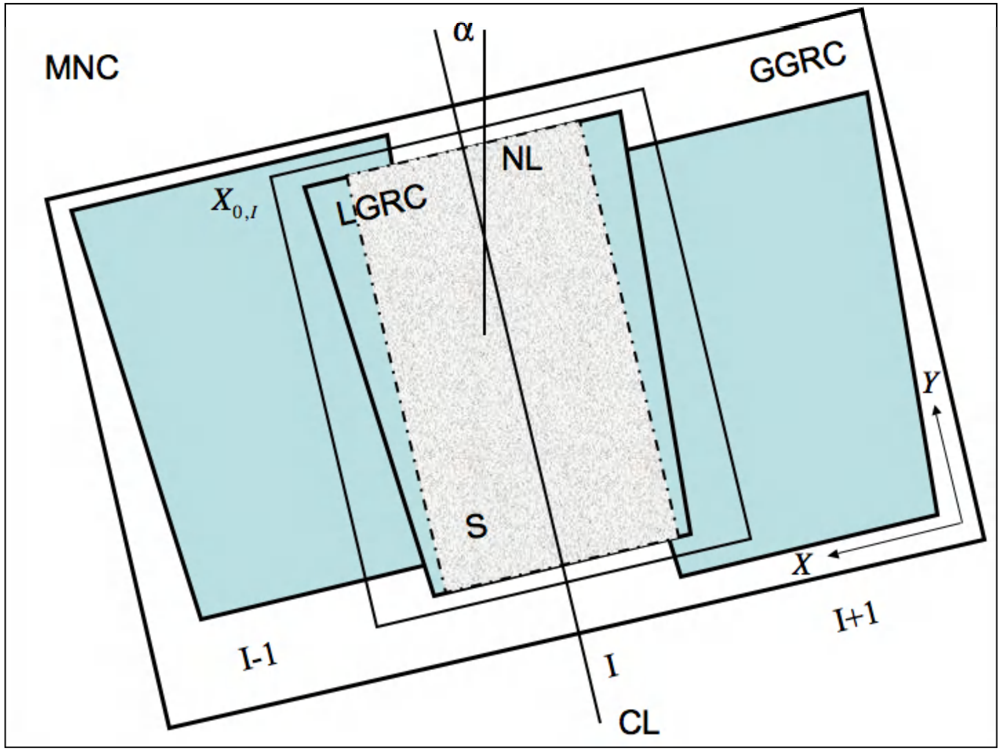

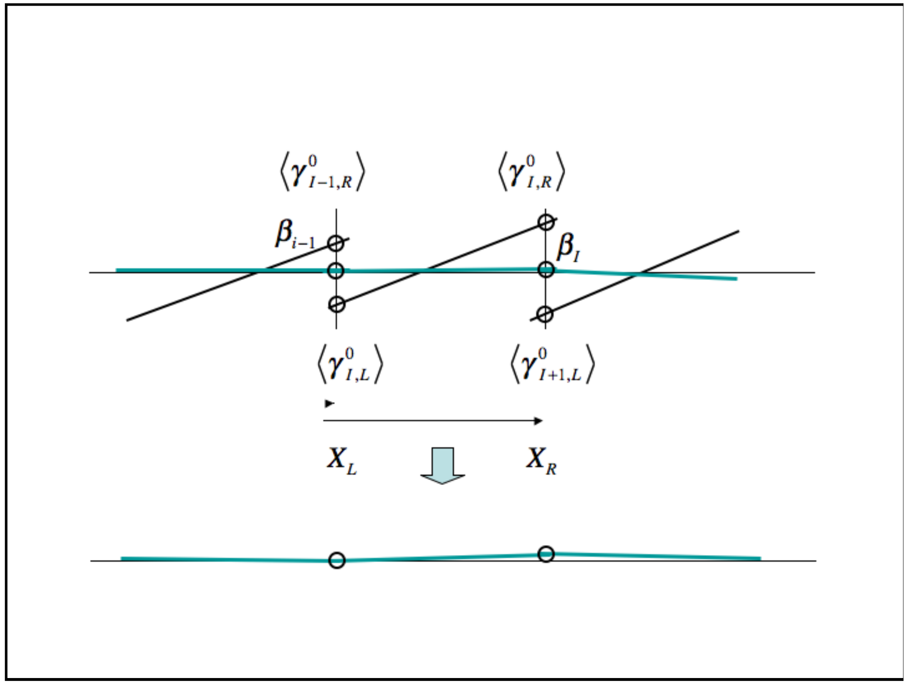

RSP410パス図
60
40
20
0
-20
-40
40
60
80
100
120
140
160
180
-160
Riau
RSP410
Australia
Browse Product

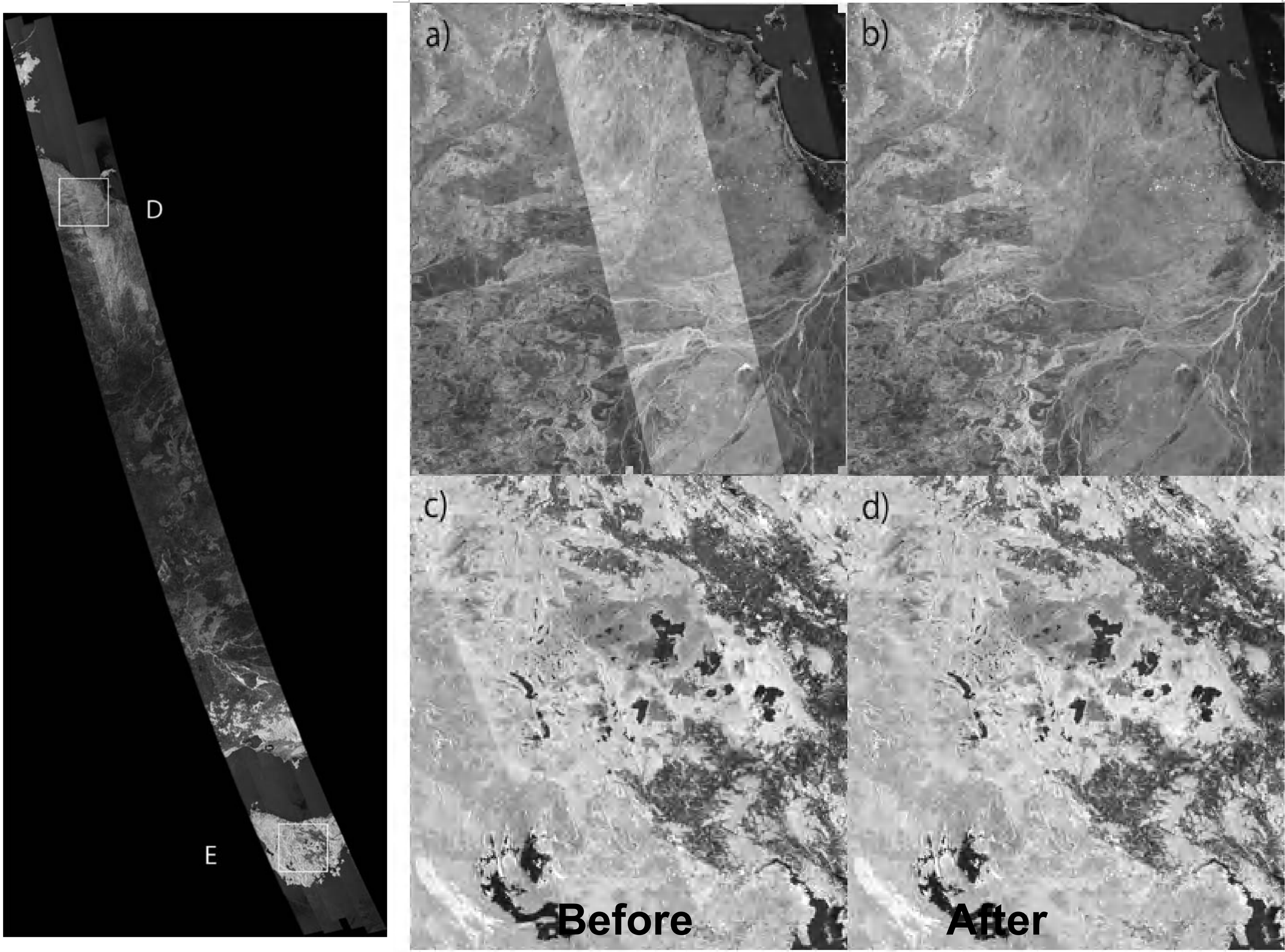
D
E
a)
b)
c)
d)
Before
After

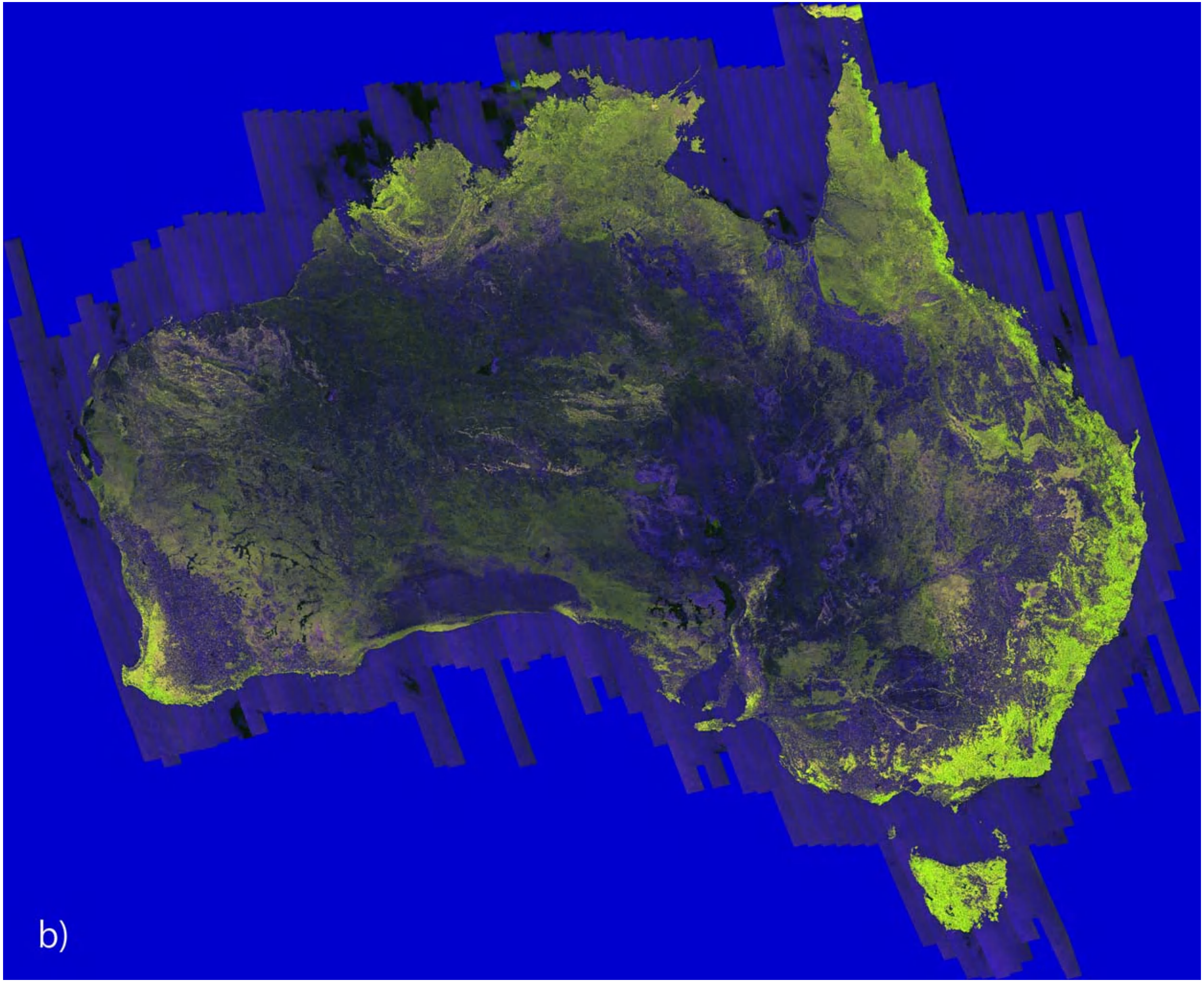

b)

Geometric accuracies

Co-registration: 0.261,0.277

Accuracy: 34.14: Landsat-mosaic
Accuracy: 11.00:CR-mosaic

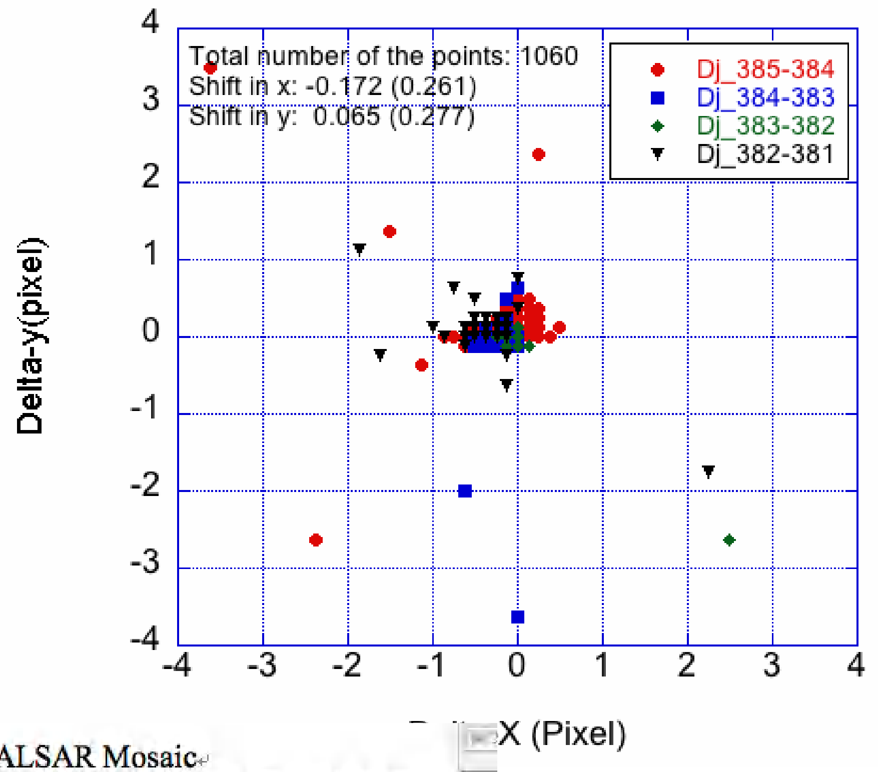

Table IV Summary of Geolocation RMSE of the JAXA PALSAR Mosaic

Area	Northing RMSE (m)	Easting RMSE (m)	Total RMSE (m)	No. of GCPs
Japan (2007)	22.81(-112.9,43.8)	34.20(-114.2,69.9)	41.11(0.0,119.3)	104
Borneo-Jawa (2007)	23.13(-76.7,71.1)	32.15(-94.5,49.4)	39.61(0.0,98.0)	104
Sumatra (2007)	27.98(-96.9,65.8)	30.03(-86.3,60.7)	41.05(0.0,129.8)	70
Philippine (2007)	17.19(-35.67,35.66)	16.86(-26.89,33.23)	24.08(0.48,43.56)	49
Philippine (2009)	22.83(-54.90,74.90)	29.34(-75.18,39.54)	37.17(0.02,98.39)	101
Borneo-Jawa (2009)	24.79(-62.75,71.95)	30.23(-79.32,26.33)	39.09(0.0,85.42)	83
Sumatra (2009)	26.42(-50.9,67.1)	32.99(-131.9,39.7)	42.26(0.0,131.9)	83
Japan (2009)	26.46(-55.8,52.3)	33.26(-90.0,61.3)	42.50(0.0,99.8)	69
Indochina (2009)	27.96(-52.5,72.9)	30.60(-92.8,75.5)	41.45(0.0,118.0)	89
Central Africa (2008)	24.30(-46.7,47.4)	21.16(-48.2,42.3)	32.22(2.9,63.0)	131
Central Africa (2009)	16.52(-35.17,30.81)	16.20(-39.16,35.88)	23.14(2.73,44.36)	147
Sulawesi (2007)	17.01(-35.14,31.79)	15.44(-30.68,37.59)	22.98(2.30,43.27)	68
Sulawesi (2009)	15.38(-33.76,33.74)	16.21(-41.20,34.76)	22.35(0.85,45.16)	67
Australia (2009)	19.66(-44.41,30.90)	18.91(-41.28,48.26)	27.28(2.35,58.44)	218
All	22.35	25.81	34.14	1393

Note: The numbers in brackets represent the minimum and maximum values respectively.

Global Observation Scenario

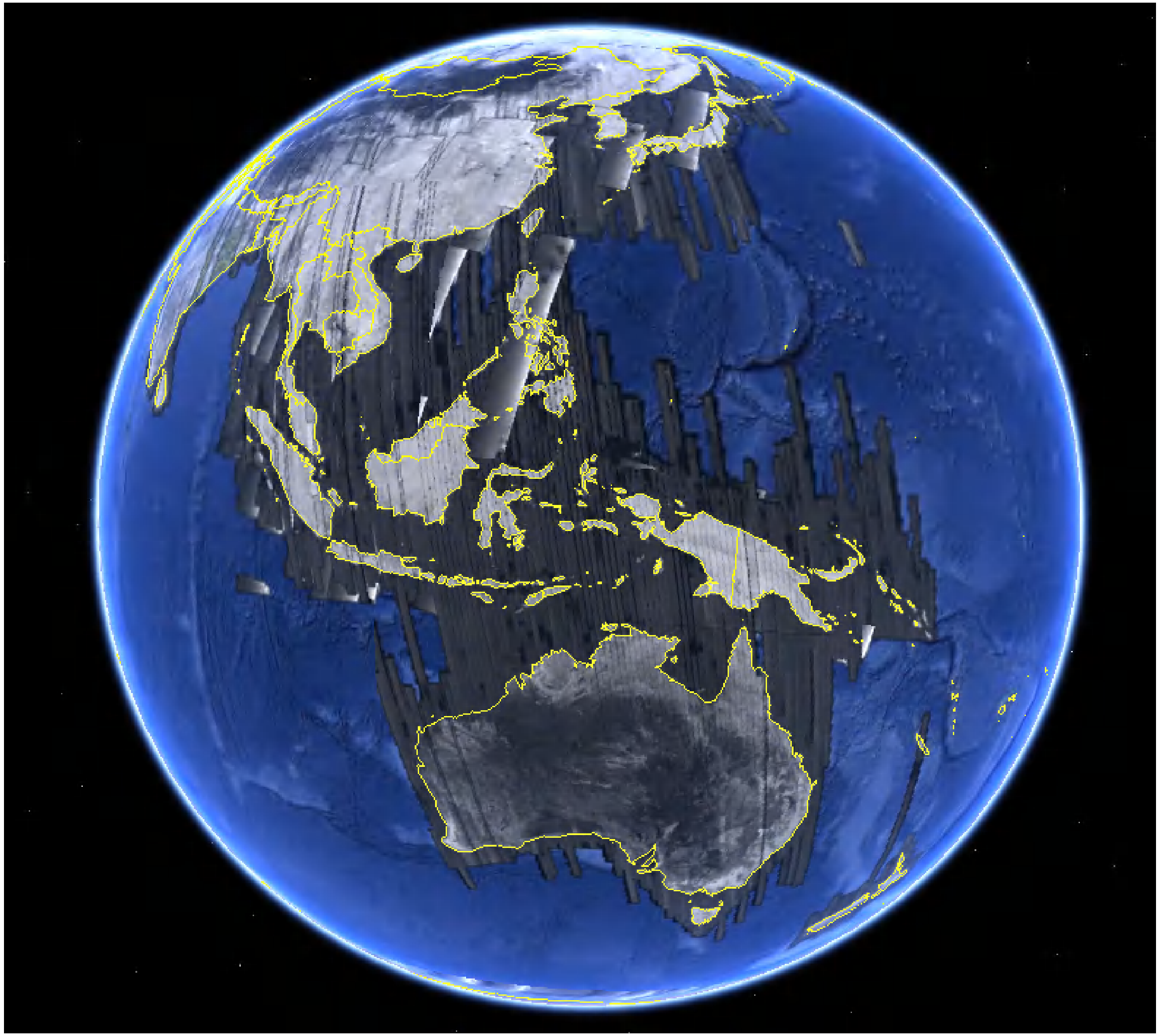

High resolution wall-to-wall observation

PALSAR
AVNIR-2
PRISM

Systematic, time-space consistent observations
46 days acquisition: (I.e., July 28 2009~ Sept. 11, 2009)

陸域観測技術衛星「だいち」(ALOS)搭載のLバンド合成開口レーダ(PALSAR；パルサー)によるパキスタンの大雨の緊急観測結果(3), Aug. 24, 2010

1) Sami Village
2) Multan
3) Faisalbad

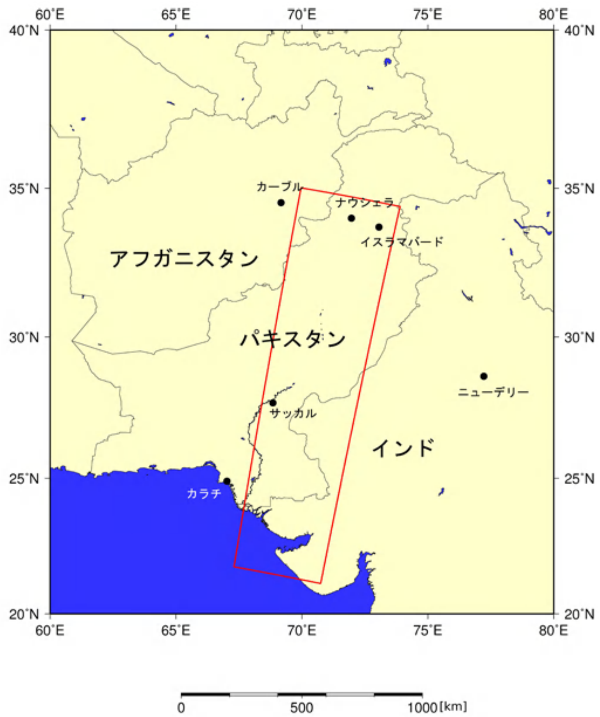

350km

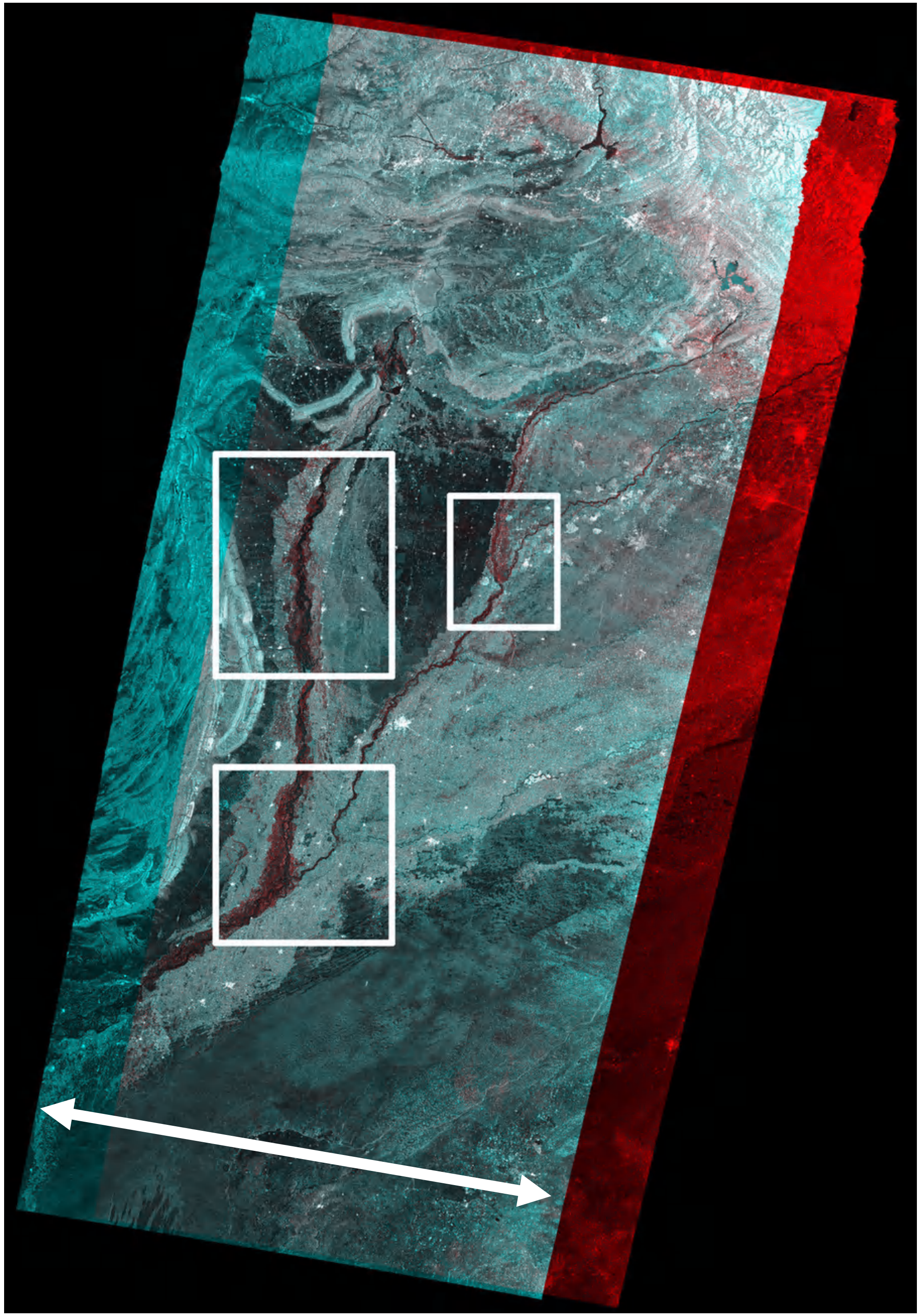

Temporal Change of the flooded basin in Pakistan

8/5-7/19, 2010

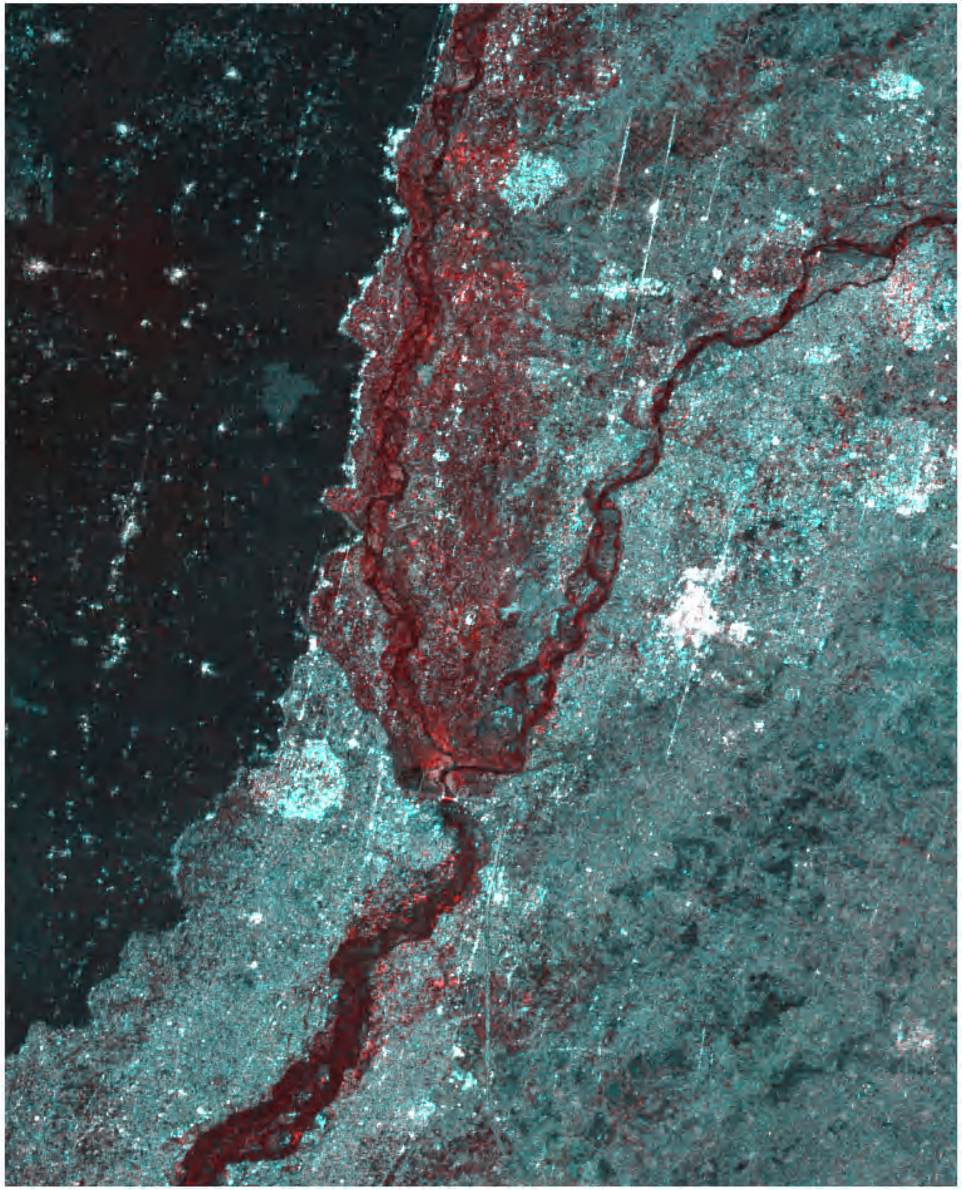

8/22-7/19, 2010

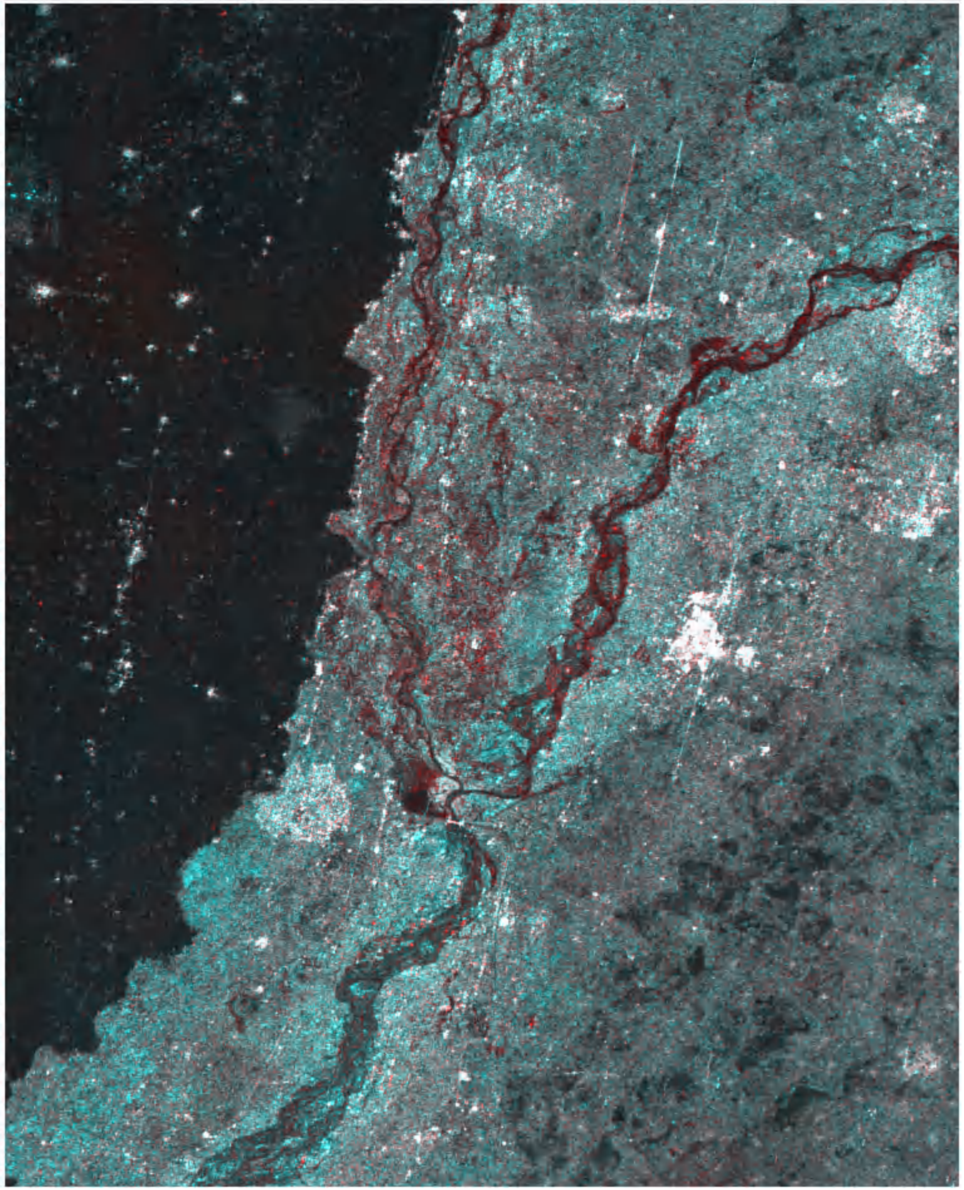

8/5-7/19, 2010

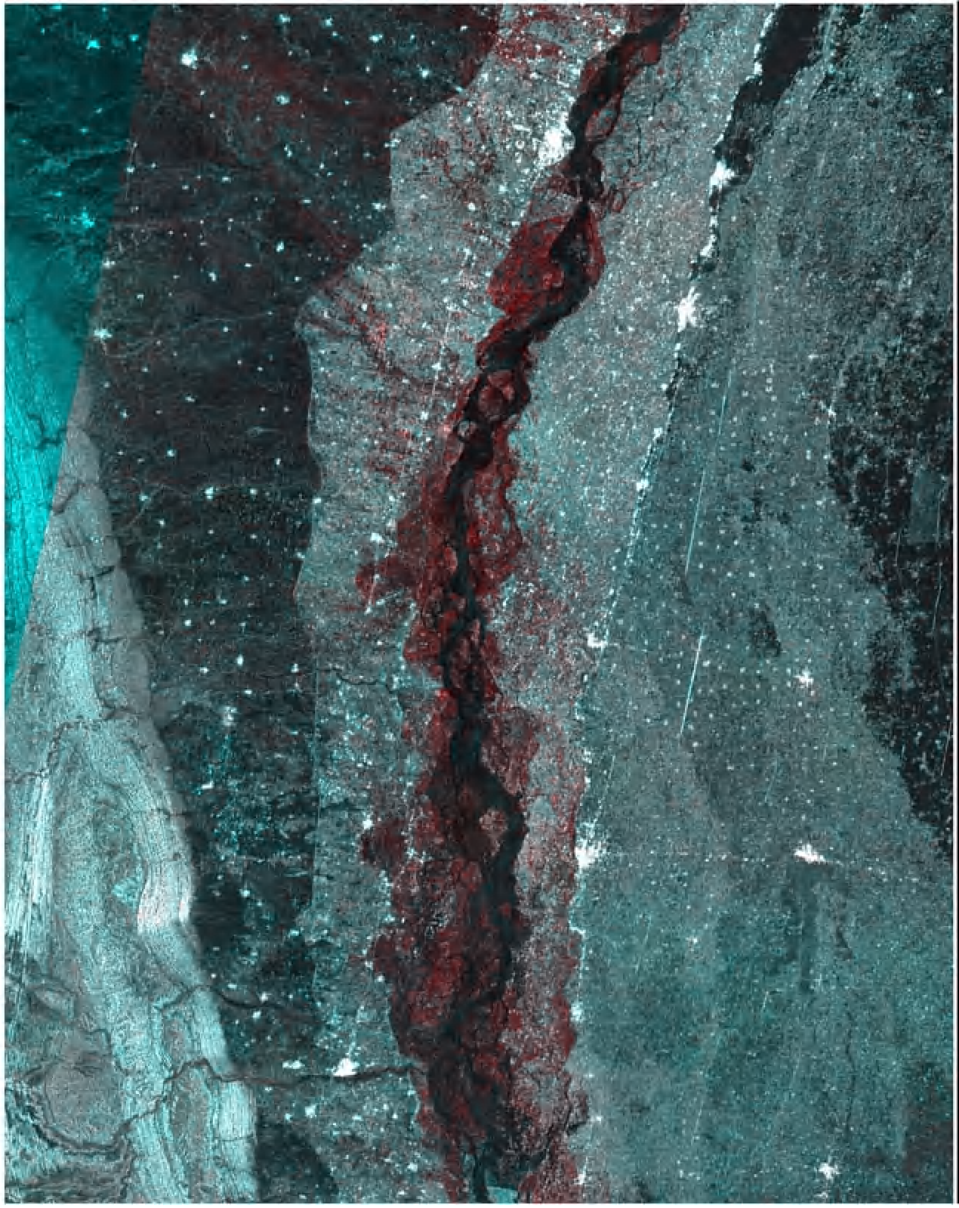

8/22-7/19, 2010

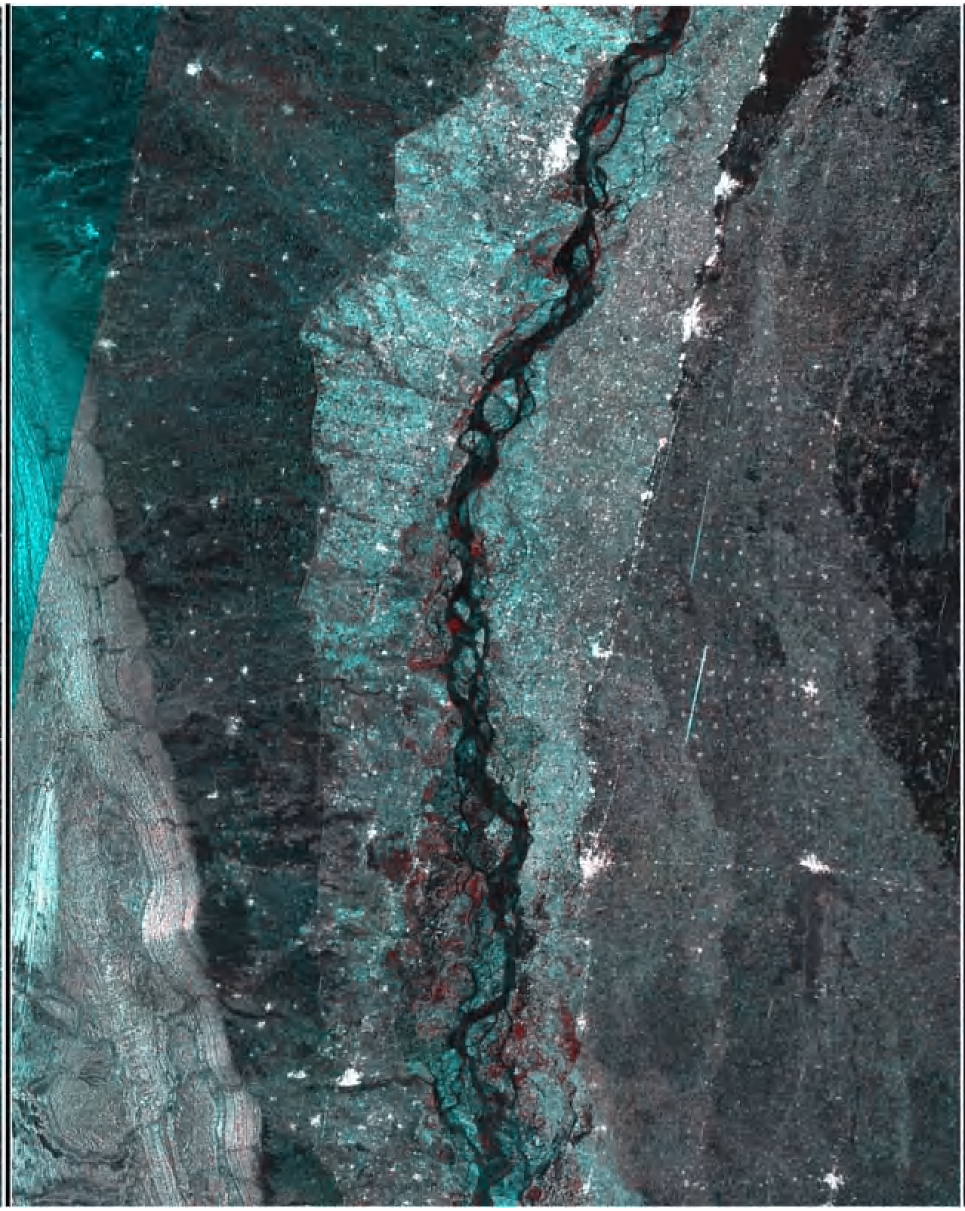

8/5-7/19, 2010

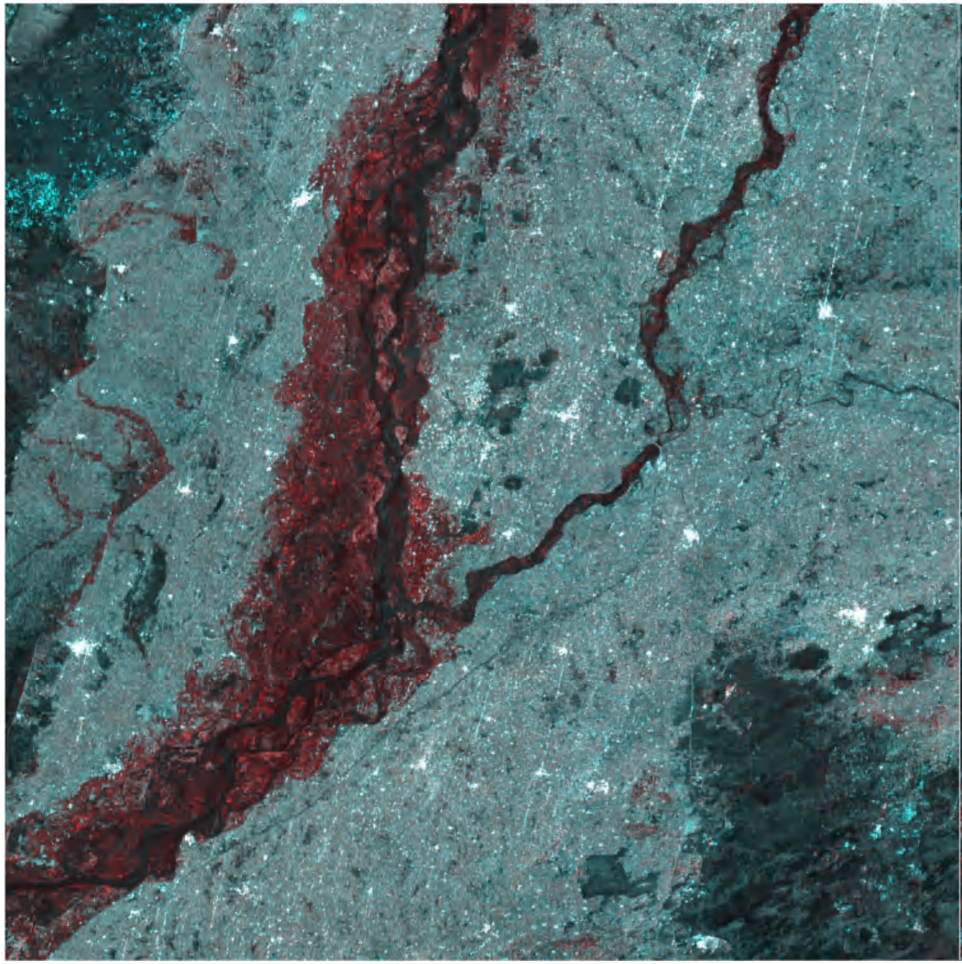

8/22-7/19, 2010

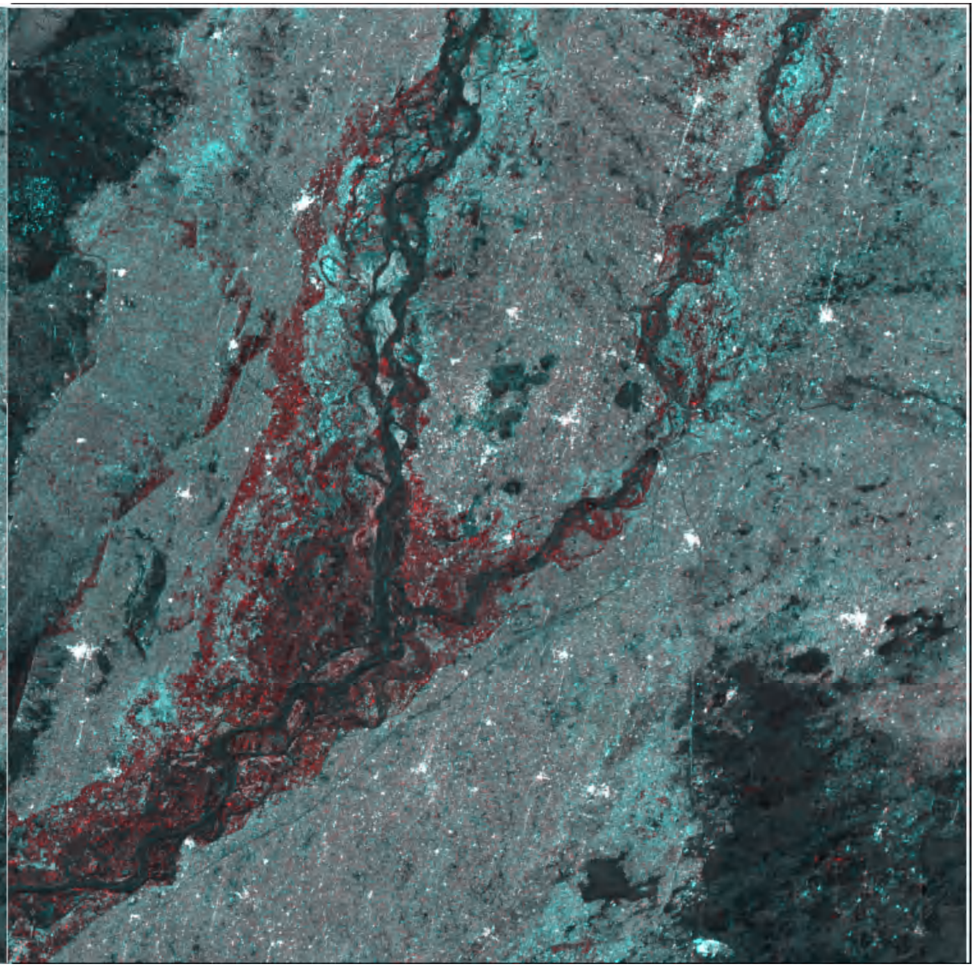

陸域観測技術衛星「だいち」(ALOS)搭載のLバンド合成開口レーダ(PALSAR;パルサー)によるパキスタンの大雨の緊急観測結果

Aug. 19, 2010

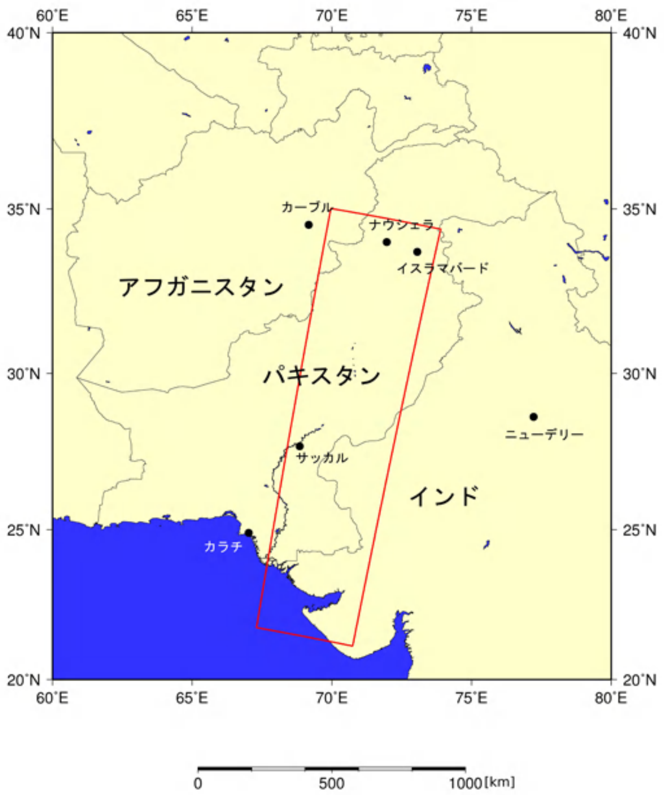

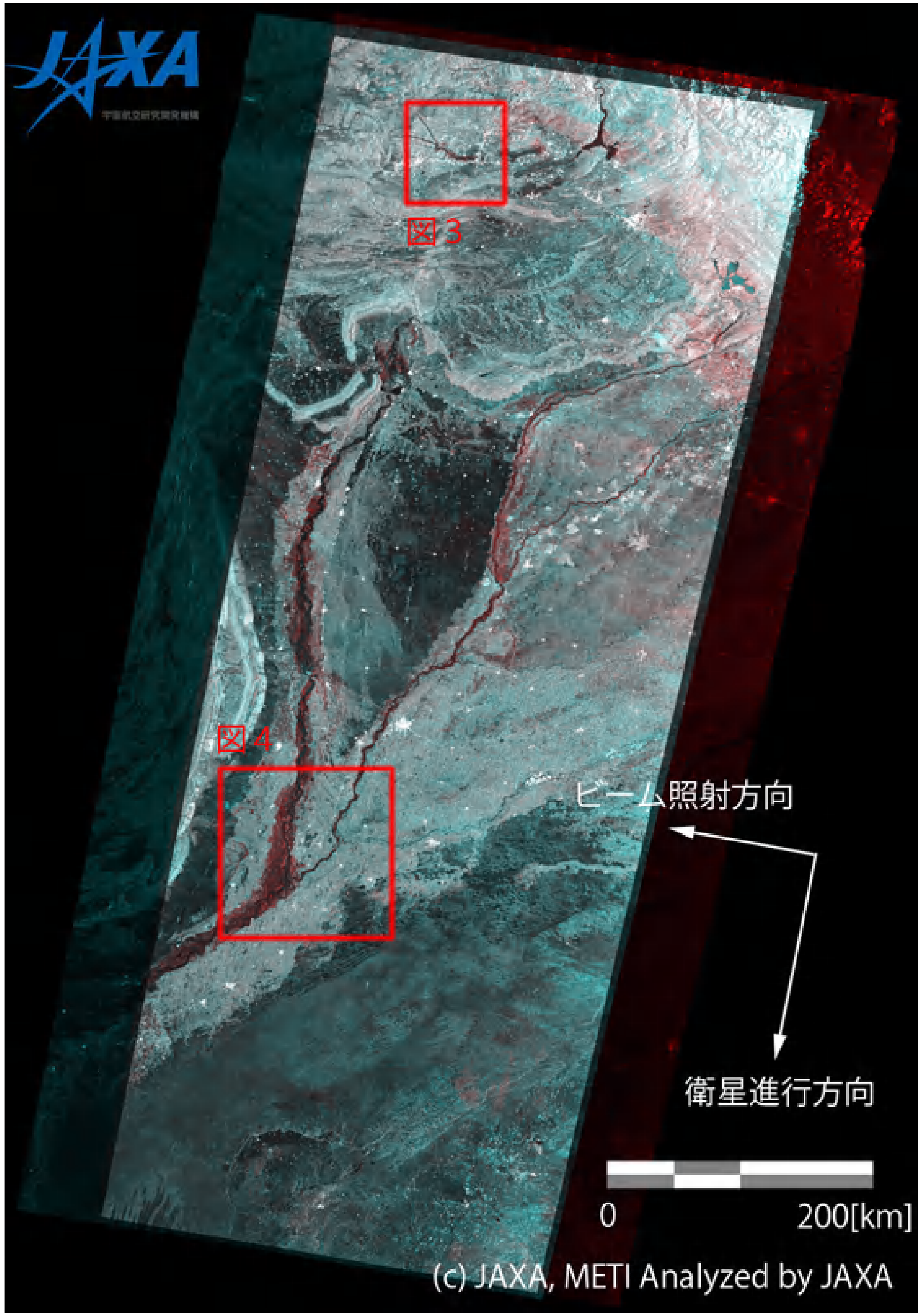

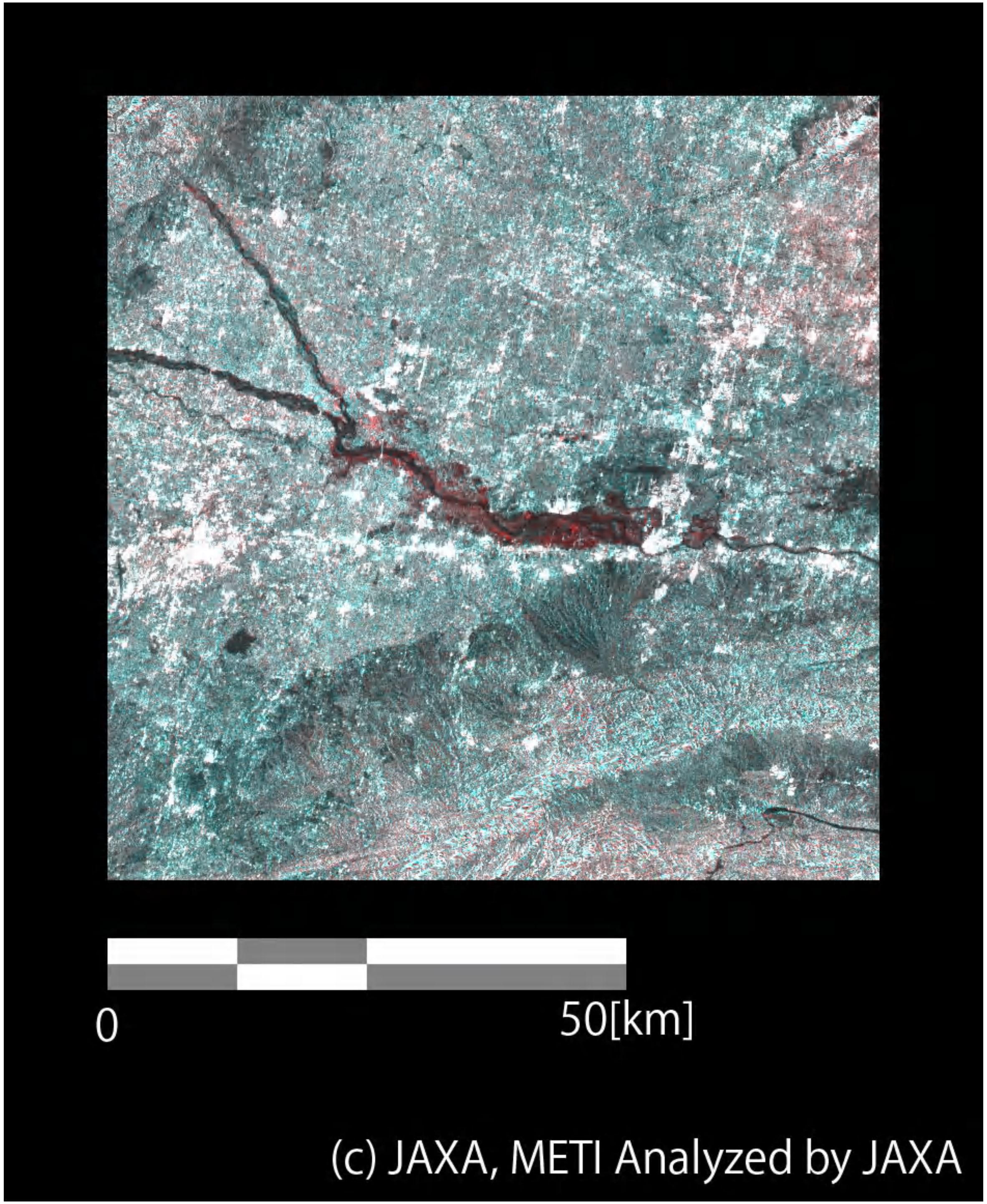
0
50[km]
(c) JAXA, METI Analyzed by JAXA

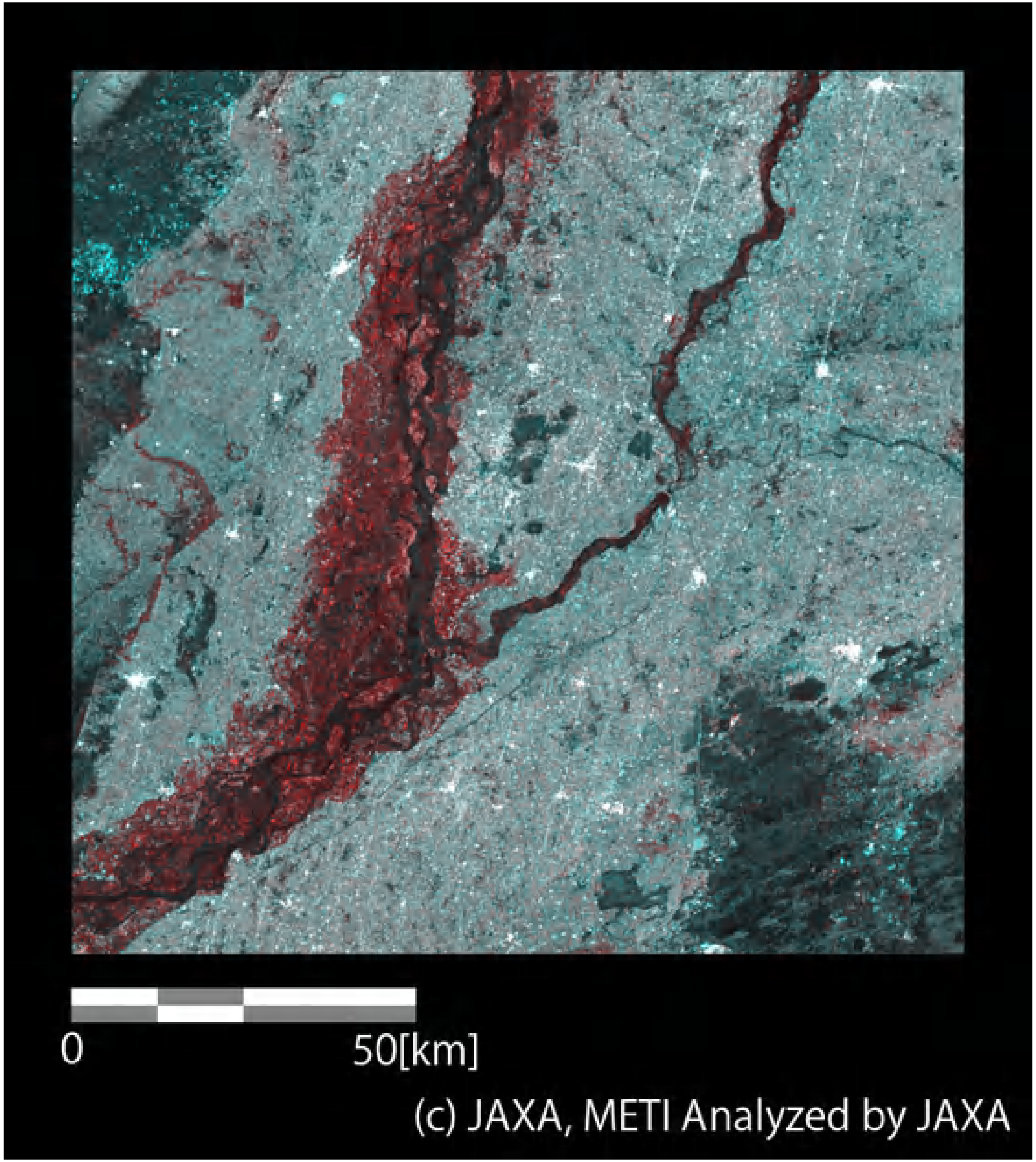
0
50[km]
(c) JAXA, METI Analyzed by JAXA

Flood monitoring for Pakistan Heaven rain from July/End 2010.

PALSAR ScanSAR in HH polarization

Precise Co-registration of the before (Red) and after (Green and Blue) the flooding in two colors

Red: flooding and no or less signal backscatter (Aug. 5~ Aug. 29 2010, 6 strips)

Blue: increase of back scatter (June 27~July 19, 2010, 6 strips)

Ortho-slope corrected gamma-zero images

ALOS/PALSAR
ScanSAR image mosaics over the Pakistan and Detection of Flooded areas

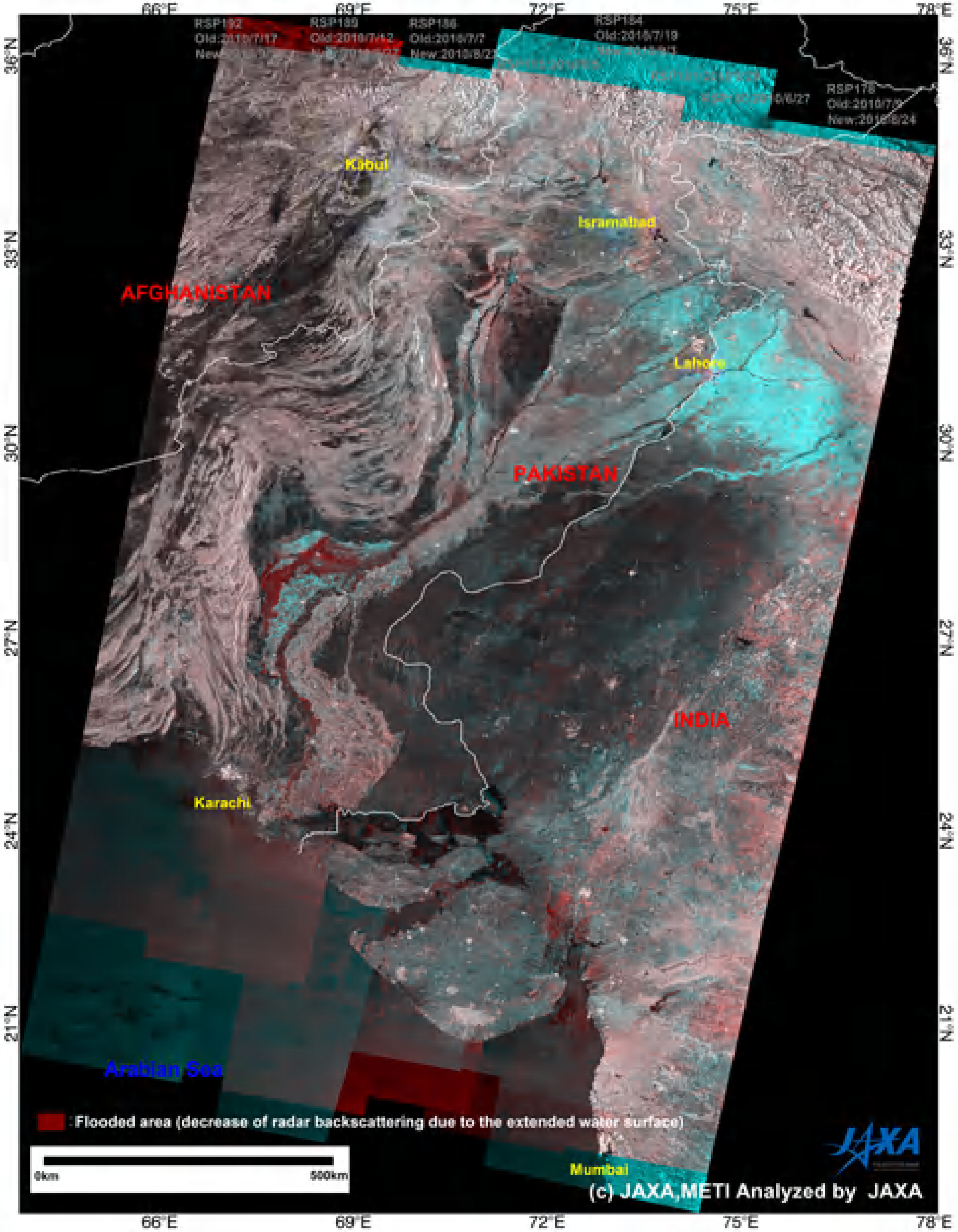

Oil Spill Monitoring at Gulf of Mexico

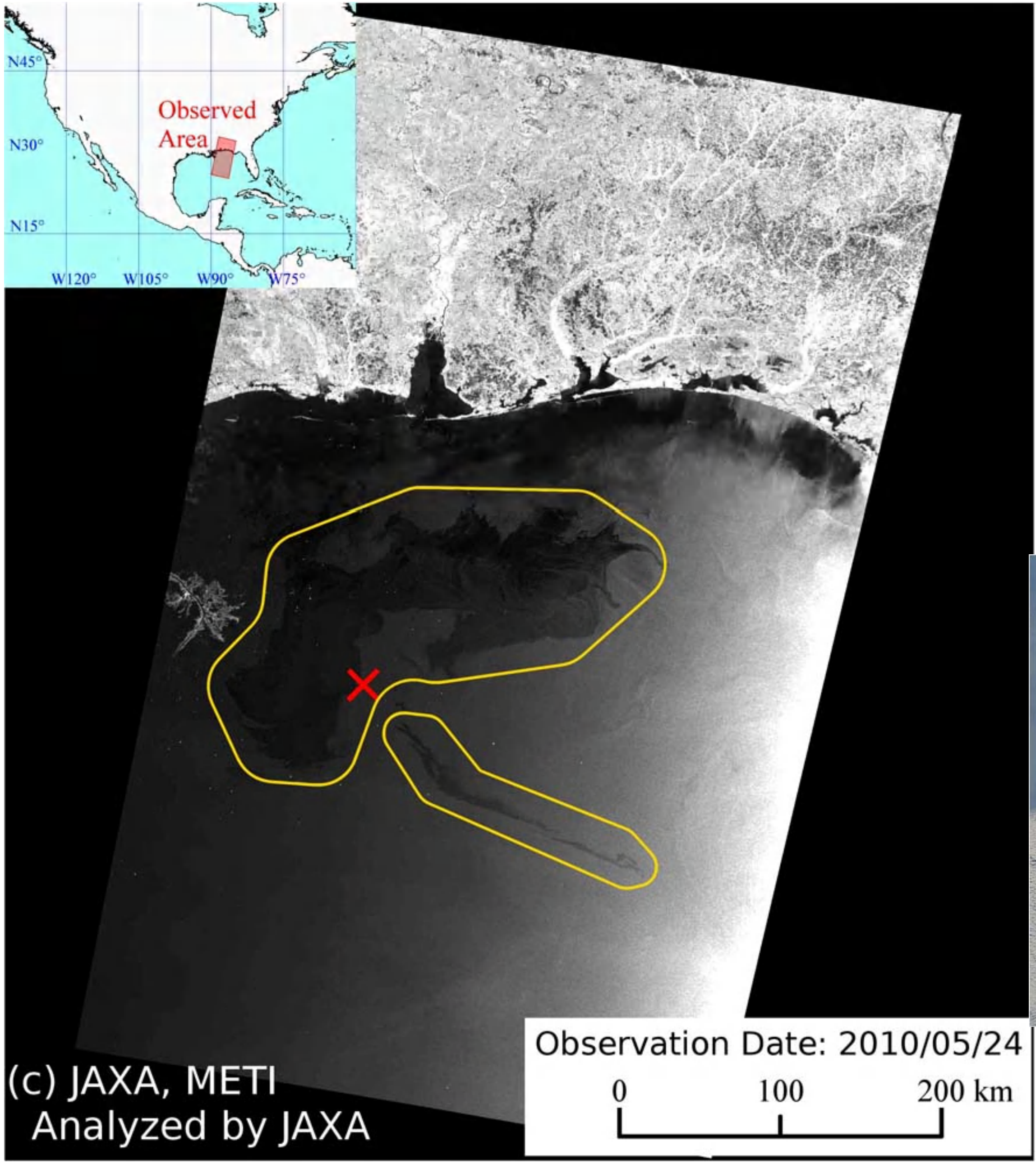

Oil Spill of Gulf of Mexico occurred on April 2010 has lasted for five months. More than ?? Of Oil were exosured on these areas.

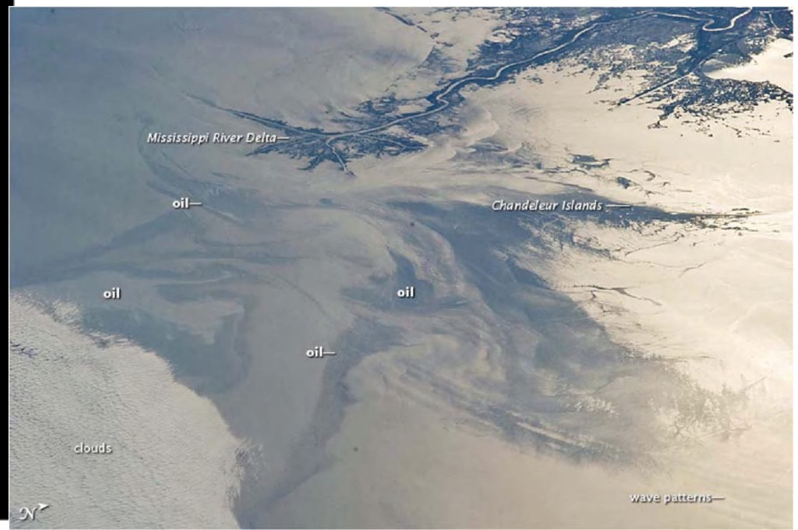

Conclusion

PALSAR has high sensitivity to the disaster monitoring.

Slope-correction, ortho-rectification, mosaicking, and multi-time overlay processing can perform the change detection of the disaster area.

Insensitivity for the weather condition at ALOS/PALSAR can support the disaster mitigation.